

Atomic structure and collision dynamics with highly charged ions

Xinwen Ma(马新文), Shaofeng Zhang(张少锋), Weiqiang Wen(汶伟强), Zhongkui Huang(黄忠魁), Zhimin Hu(胡智民), Dalong Guo(郭大龙), Junwen Gao(高俊文), Bennaceur Najjari, Shenyue Xu(许慎跃), Shuncheng Yan(闫顺成), Ke Yao(姚科), Ruitian Zhang(张瑞田), Yong Gao(高永), and Xiaolong Zhu(朱小龙)

Citation: Chin. Phys. B, 2022, 31 (**9**): 093401. DOI: 10.1088/1674-1056/ac8736
Journal homepage: http://cpb.iphy.ac.cn; http://iopscience.iop.org/cpb

What follows is a list of articles you may be interested in

Electron-impact ionization cross section calculations for lithium-like ions

Guo-Jie Bian(卞国杰), Jyh-Ching Chang(张稚卿), Ke-Ning Huang(黄克宁), Chen-Sheng Wu(武晨晟), Yong-Jun Cheng(程勇军), Kai Wang(王凯), and Yong Wu(吴勇)

Chin. Phys. B, 2022, 31 (**1**): 013401. DOI: 10.1088/1674-1056/ac229e

Multiple recollisions in nonsequential double ionization below the recollision-ionization threshold

Xiao-Meng Ma(马晓萌), Ai-Hong Tong(童爱红), Zhuo Wang(王茁), and Chun-Yang Zhai(翟春洋)

Chin. Phys. B, 2021, 30 (**12**): 123402. DOI: 10.1088/1674-1056/ac2d1e

Enhancement of electron-ion recombination rates at low energy range in the heavy ion storage ring CSRm

Nadir Khan, Zhong-Kui Huang(黄忠魁), Wei-Qiang Wen(汶伟强), Shu-Xing Wang(汪书兴), Han-Bing Wang(汪寒冰), Wan-Lu Ma(马万路), Xiao-Long Zhu(朱小龙), Dong-Mei Zhao(赵冬梅), Li-Jun Mao(冒立军), Jie Li(李杰), Xiao-Ming Ma(马晓明), Mei-Tang Tang(汤梅堂), Da-Yu Yin(殷达钰), Wei-Qing Yang(杨维青), Jian-Cheng Yang(杨建成), You-Jin Yuan(原有进), Lin-Fan Zhu(朱林繁), Xin-Wen Ma(马新文)

Chin. Phys. B, 2020, 29 (**3**): 033401. DOI: 10.1088/1674-1056/ab69eb

Theoretical investigations of collision dynamics of cytosine by low-energy (150-1000 eV) proton impact

Zhi-Ping Wang(王志萍), Feng-Shou Zhang(张丰收), Xue-Fen Xu(许雪芬), Chao-Yi Qian(钱超义)

Chin. Phys. B, 2020, 29 (**2**): 023401. DOI: 10.1088/1674-1056/ab6313

Charge state effect on the K-shell ionization of iron by xenon ions near the Bohr velocity

Zhou Xian-Ming, Zhao Yong-Tao, Ren Jie-Ru, Cheng Rui, Lei Yu, Sun Yuan-Bo, Xu Ge, Wang Yu-Yu, Liu Shi-Dong, Xiao Guo-Qing

Chin. Phys. B, 2013, 22 (**11**): 113402. DOI: 10.1088/1674-1056/22/11/113402

TOPICAL REVIEW — Celebrating 30 Years of *Chinese Physics B*

Atomic structure and collision dynamics with highly charged ions

Xinwen Ma(马新文)[1,2,3,†], Shaofeng Zhang(张少锋)[1,2], Weiqiang Wen(汶伟强)[1,2], Zhongkui Huang(黄忠魁)[1,2], Zhimin Hu(胡智民)[4], Dalong Guo(郭大龙)[1,2], Junwen Gao(高俊文)[5], Bennaceur Najjari[1], Shenyue Xu(许慎跃)[1,2], Shuncheng Yan(闫顺成)[1,2], Ke Yao(姚科)[6], Ruitian Zhang(张瑞田)[1,2], Yong Gao(高永)[1,2], and Xiaolong Zhu(朱小龙)[1,2]

[1] *Institute of Modern Physics, Chinese Academy of Sciences, Lanzhou* 730000, *China*
[2] *University of Chinese Academy of Sciences, Beijing* 100049, *China*
[3] *Key Laboratory of Atomic and Molecular Physics and Functional Materials of Gansu Province, College of Physics and Electronic Engineering, Northwest Normal University, Lanzhou* 730070, *China*
[4] *Key Laboratory of Radiation Physics and Technology of the Ministry of Education, Sichuan University, Chengdu* 610064, *China*
[5] *Department of Physics, Hangzhou Normal University, Hangzhou* 311121, *China*
[6] *Shanghai EBIT Laboratory, Key Laboratory of Nuclear Physics and Ion-Beam Application (MOE), Fudan University, Shanghai* 200433, *China*

(Received 1 June 2022; revised manuscript received 3 August 2022; accepted manuscript online 5 August 2022)

The research progresses on the investigations of atomic structure and collision dynamics with highly charged ions based on the heavy ion storage rings and electron ion beam traps in recent 20 years are reviewed. The structure part covers test of quantum electrodynamics and electron correlation in strong Coulomb field studied through dielectronic recombination spectroscopy and VUV/x-ray spectroscopy. The collision dynamics part includes charge exchange dynamics in ion–atom collisions mainly in Bohr velocity region, ion-induced fragmentation mechanisms of molecules, hydrogen-bound and van de Waals bound clusters, interference, and phase information observed in ion–atom/molecule collisions. With this achievements, two aspects of theoretical studies related to low energy and relativistic energy collisions are presented. The applications of data relevant to key atomic processes like dielectronic recombination and charge exchanges involving highly charged ions are discussed. At the end of this review, some future prospects of research related to highly charged ions are proposed.

Keywords: highly charged ion, atomic structure, collision dynamics, quantum electrodynamics, fragmentation mechanisms, relativistic effects, electron correlation

PACS: 34.70.+e, 34.50.–s, 36.40.Qv, 34.80.Lx **DOI:** 10.1088/1674-1056/ac8736

1. Introduction

The invention of quantum mechanics and special relativity have already deepened our understanding of the nature of the world and been promoting the developments of physics, chemistry, astronomy as well as applied sciences. Their combination is the foundation for the birth of quantum electrodynamics (QED), the most accurate and successful theory in physics to date, which is the basis of modern field theories that constitute the current standard model. In the last 70 years, the theories have been tested with high precision in the light atomic system, especially in atomic hydrogen,[1] where electron moves in a weak electromagnetic field where perturbative approximation is sufficient. However, early in the 1930s, scientists like Schwinger and Heisenberg have already pointed out that novel phenomena may appear when an electron moves in extremely strong fields. Highly charged ions (HCIs) can provide such extreme conditions in heavy atomic systems. For example, the 1s orbital electron of uranium ion experiences an average electric field of 1×10^{16} V/cm, which is six orders of magnitude stronger than that in atomic hydrogen. Such a strong field could not be macroscopically generated in the laboratory.

With the advent of heavy-ion storage rings[2] and electron beam ion trap (EBIT),[3] HCIs such as bare-, hydrogen-, and lithium-like xenon and lead, can be produced efficiently and used for experimental studies. For storage rings based on accelerator facilities, the HCIs are produced through stripping techniques by accelerating low-charged ions up to energies high enough, while in EBITs, HCIs are generated by ionization of atoms with high energy electron impacts. Significant progresses in the studies of the structure and dynamics of heavy highly charged ions have been made in past decades. However, in the former case, one of the major challenge in precision measurements with high energy HCIs is the uncertainty caused by the Doppler effects. In the latter case, the challenge comes from the statistical uncertainty due to the very limited number of heavy HCIs trapped in EBITs. In both cases, experiments of structure studies involve photon spectroscopy and resonant collision spectroscopy. Photon spectroscopy detects direct photons or cascade photons from electron capture recombination processes. In parallel, at the electron cooler of the storage rings, resonant collision spectroscopy, also called dielectronic recombination spectroscopy (DR spectroscopy),

[†]Corresponding author. E-mail: x.ma@impcas.ac.cn

© 2022 Chinese Physical Society and IOP Publishing Ltd

has been developed into a new, high precision and highly efficient spectroscopic tool for HCIs by detecting the combined ions instead of photons. For the technical details, we refer the reader to the paper by Mokler.[4]

In contrast to the situation in studies of the stationary atomic system which has been described by the quantum mechanics with unprecedented precision, our knowledge of the dynamical few-body system is still far from satisfactory. Understanding and minimizing the differences between theory and experiment remains a major challenge in the field. For instance, the discrepancies in the fully differential cross-sections of the single ionization of helium by bare C^{6+} projectile between experimental data and theoretical models were reported in 2003 which remains one of the major puzzles nowadays.[5] However, in atomic systems the interaction potential between charged particles is exact and all discrepancies between experiments and theories can thus be attributed to the few-body dynamic problem.[6] Knowledge of few-body dynamics plays a crucial role in solid physics, chemical reaction, biological systems, and so on since all the structure and evolution of the macroscopic world is to a large extent governed by these rules.[6,7]

Accelerators provide the access to the studies of ion-atom/molecule/cluster collisions with various impact velocities. A major breakthrough has occurred since the invention of the cold target recoil ion momentum spectrometer (COLTRIMS).[5] or reaction microscope.[6] For the first time, fully differential cross sections are accessible for charge exchange and ionization processes. Various mechanisms in ion–atom collisions have been identified, such as the so-called Thomas transfer and ionization mechanism,[8] saddle point ionization mechanism,[9] quasimolecular electron promotion mechanism,[10] electron-correlation mediated doubly excited state population involving keV highly charged ions,[11,12] equivalent "photon ionization" in 1 GeV/u U^{92+} single ionization collision with He,[13] to name just a few. Also, the technique has been applied in photon-atom interactions based on ultrafast lasers and synchrotron radiation, for example, the nonsequential double ionization mechanism in a strong laser field,[14,15] the quasi-free mechanism for single-photon double ionization at 440 eV and 800 eV,[16] and Compton scattering at low photon energy,[17] *etc.* Recent striking theoretical progress in the atomic orbital close coupling approach is manifested in the description of inelastic electronic processes involving one and two electrons in the intermediate energy domain.[18] When a molecular target is used, more freedoms, such as fragmentation paths and the orientation of the molecular axis in space, will be involved, and new fragmentation mechanisms induced by HCIs have been revealed.[19,20] Recently, progresses in studies of quantum grating as well as phase information obtained in ion-molecule collisions render us new opportunities to explore principles underlying the non-local realism and deeper information in fundamental quantum processes.[21,22]

Radiative transition and charge exchange collisions also play crucial roles in various fundamental and applied fields,[8] such as astrophysics, fusion plasma physics and radiotherapy. The understanding and modeling of the phenomena in energy loss, charge balance and diagnostics of plasma properties rely largely on accurate collision cross sections provided by laboratory charge exchange measurements. For all these purposes, benchmark atomic data are required.

The research related to HCIs is extraordinarily extensive, and of course, it will be too ambitious to cover all achievements in one review paper. Therefore, from our perspective, this review will mainly report and review the most significant progresses of precision spectroscopy and collision dynamics with highly charged ions related to storage rings and EBITs in recent 20 years and some applications in astrophysics as well as fusion plasma diagnostic and modeling will also be discussed. Finally, a summary will be presented and some future aspects are proposed.

2. Precision spectroscopy of HCIs

Dielectronic recombination (DR) is a resonant recombination process, in which a free electron is captured into an ion with one of its inner-shell electrons excited simultaneously. DR is a two-step process as schematically shown in Fig. 1, *i.e.*, in the first step, a free electron is captured into L-shell by an ion A^{q+} with a K-shell bound electron, the excess energy is directly transferred to excite one K-electron (resonant condition is required), by which an intermediate doubly excited state of the ion is formed $A^{(q-1)+**}(LL')$ $((a) \rightarrow (b))$. In the second step, the doubly excited state decays radiatively to states below the auto-ionization threshold $((b) \rightarrow (c))$, and the emitted photon could be recorded for spectroscopic purposes. DR is sensitive to atomic levels and has been developed as high precision spectroscopy at storage rings. Radiative recombination (RR) occurs non-resonantly when a free electron is captured into a bound state of the ion and emits a photon directly.

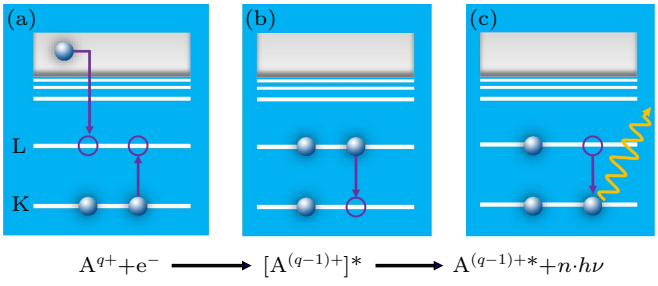


Fig. 1. Schematic diagram of the KLL-DR process of He-like ions.

DR is one of the most important and fundamental electronion–ion collision processes in hot plasmas and it can

significantly affect the ionization balance and energy-level population of hot plasmas. Furthermore, DR strongly modifies the properties of radiation from hot plasmas because the doubly excited states formed in the DR process are mainly stabilized by radiative decay rather than Auger decay, especially for highly charged heavy ions. In addition, the intensities of dielectronic satellite lines are sensitive to environmental temperature and density, which are of great significance in diagnosing the properties of hot plasmas in astrophysics[23] and fusion science.[24] DR also plays an important role in fundamental research and has been used in studying QED effects in few-electron ions,[25] isotope shift,[26] hyperfine quenching,[27] and hyperfine splitting.[28]

2.1. DR spectroscopy at storage rings

Storage rings equipped with an electron cooler provide a uniquely effective technique to obtain accurate spectroscopy and determine absolute DR rate coefficients. There are two main motivations for DR studies of HCIs at heavy-ion storage rings. (i) Precise DR spectroscopy provides accurate atomic structure data for test of QED, electron correlation, relativistic, and nuclear effects. (ii) The measured absolute DR rate coefficients provide benchmark data for understanding the astrophysical and other natural as well as man-made plasmas.[29] In the last decades, a series of DR experiments with HCIs have been carried out at the storage rings, for examples, test storage ring (TSR) at Max-Planck-Institut für Kernphysik (MPIK) in Heidelberg,[30] experimental storage ring (ESR) at GSI in Darmstadt,[31] CRYRING at MSL in Stockholm.[32]

The DR experiments performed at CRYRING in Stockholm mainly employed relatively light heavy ions ($Z \leq 18$) with charge states less than $q = 10+$ due to the performance of its ion source, including C^{q+}, N^{q+}, O^{q+} ($q = 3,4,5$), F^{r+}, Ne^{r+}, S^{r+}, Ar^{r+} ($r = 5,6,7$), Si^{3+}, and Si^{10+}, *etc.* All these works measured the DR spectra and obtained the resonance positions and the rate coefficients which are of interest for astrophysics. Only three heavier ions are used for DR spectroscopic studies with high precision. Mg-like Ni^{17+} ions were measured in the energy range up to 6.5 eV, the $3s_{1/2}$–$3p_{1/2}$ and the $3s_{1/2}$–$3p_{3/2}$ ($\Delta n = 0$) energy splittings were determined from the experiments and compared with the relativistic many-body perturbation theory calculation. For Li-like Kr^{33+} ions, the ($2s_{1/2}$–$2p_{1/2}$) Lamb shift was obtained. For Cu-like Pb^{53+} ions, DR resonances were identified in the very low relative energy range of $\sim 10^{-3}$ eV–10^{-4} eV. The Pb^{53+} ($4p_{1/2}$–$4s_{1/2}$) energy splitting of ~ 118 eV is determined with an accuracy of about 10^{-3} eV, which provides a test of QED in a many-body environment. In addition, precise determination of the $4s_{1/2}$ and $4p_{1/2}$ levels for the two isotopes of $^{208,207}Pb^{53+}$ demonstrated the potential of DR spectroscopy to measure isotope shifts. The above works were mostly carried out before 2010, then there was a plan to combine the ESR and CRYRING along with the availability of heavy bare, one- and few-electron ions and exotic nuclei, which will open a new field of research under extreme conditions.[33] The CRYRING is already moved and installed at GSI and under commissioning presently.[33]

The heavy ion storage can employ usual thermal cathode and photon cathode to provide electron target beam. In the former case, a series of systematic DR measurements has been done focusing on the absolute dielectronic recombination rate coefficients, especially for iron and tungsten ions of particular importance for astrophysics and fusion plasma studies, see Subsection 2.4 for details. In the latter case, the DR spectra have very high precision due to the extremely low temperature of photoelectron beam.[28] Although it is a challenging task to operate the photoelectron cathode, DR spectroscopic experiments have been carried out at TSR, *e.g.* for Be-like Cl^{13+} and Ge^{28+} ions, to investigate the QED effects. The DR precision spectroscopy has been extended to investigate the nuclear properties of highly charged ions. The hyperfine splitting[28] for Li-like Sc^{18+} ($I = 7/2$, $\mu_I = 4.7565$) ions are measured and the separation of just 6 meV for the resonance states was achieved as shown in Fig. 2(a). The hyperfine quenching was studied by DR spectroscopy at TSR using Au^{20+} and Pt^{48+} ions. After 2010, it was proposed to setup the heavy-ion, low-energy ring TSR at the HIE-ISOLDE facility in CERN, Geneva, and to provide a capability for experiments with stored secondary beams that is unique in the world[34] later on, TSR stopped operation, however, due to various reasons, the plan was postponed.

The atomic research performed on ESR at GSI mainly focuses on heavy highly charged ions, x-ray spectroscopy (see Subsection 2.3) and DR spectroscopy are two of main active topics. DR spectra for Li-like ions of Xe^{51+} ($Z = 54$),[35] Pb^{79+} ($Z = 82$), Bi^{80+} ($Z = 83$), and U^{89+} ($Z = 92$)[25] have been measured and the transition energy of the 2s–2pj was extracted respectively and compared with fully relativistic multi configuration Dirac Fock (DR/MCDF) calculations. Also the DR spectra for Be-like ions of Xe^{50+} ($Z = 54$),[35] Au^{75+} ($Z = 82$), Pb^{78+} ($Z = 83$), and U^{88+} ($Z = 92$) have been measured and the relativistic effects as well as the Breit interaction in strong Coulomb field are investigated. Of particular interest are the application of DR spectroscopy to isotopes and radioactive ions produced by nuclear reaction at ESR storage ring. The measured dielectronic recombination spectra of the two Li-like neodymium isotopes $^{A}Nd^{57+}$ ($Z = 60$) with $A = 142$ (orange) and $A = 150$ (black) in the energy range of the $^{A}Nd^{56+}(1s^2 2p_{1/2} 18l_j)$ resonance group[26] are shown in Fig. 2(b), and the isotope shifts are clearly demonstrated. An exemplary DR experiment in the preparation of artificially synthesized rare isotope at the ESR storage ring is success-

fully demonstrated for $^{234}Pa^{88+}$ ($Z = 91$),[36] whose lifetime is 6.7 hours (ground state ^{234}Pa) and 1.16 minutes (isomeric state ^{234m}Pa), respectively. As a result, storage-ring DR experiments have been developed as a tool for the ultra-high precision spectroscopy of HCIs, and the access to nuclear parameters such as charge radius, spin, magnetic moment or lifetimes of long-lived excited nuclear states (isomers) become feasible employing DR technique. More details of the DR experiments at storage rings can be found in the review papers[29,30,37] and the references cited therein.

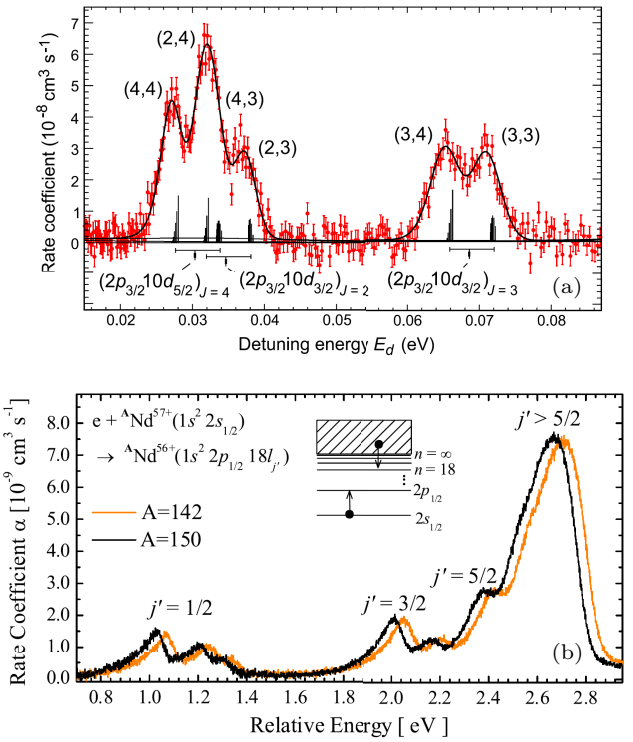


Fig. 2. (a) Hyperfine splitting of the lowest DR resonances in Li-like Sc^{18+}.[28] (b) Dielectronic recombination of the Li-like neodymium isotopes $^{142}Nd^{57+}$ (orange) and $^{150}Nd^{57+}$ (black line) in the energy range of the $1s^22p_{1/2}18l$.[26] Reproduced with permission from Refs. [26,28].

The main Cooler Storage Ring (CSRm) and the experimental Cooler Storage Ring (CSRe) at Heavy Ion Research Facility in Lanzhou (HIRFL) are both equipped with electron cooling devices, which provide ideal research platforms for DR precision spectroscopy of HCIs. Figure 3 presents the layout of the HIRFL-CSR and the main DR experimental parameters at the CSRm and the CSRe. The DR experimental method at the CSRm has been already described in detail elsewhere.[38–40] In order to perform DR experiments with high-Z HCIs, the electron cooler (EC-300) at the CSRe has been upgraded with an embedded electron energy fast detuning system for the merged-beams electron–ion collision experiments. A plastic scintillation detector (PSD) and a multi-wire proportional chamber (MWPC) detector have been developed and installed downstream of the electron cooler to detect the recombined and ionized ions in the electron-ion collision experiments at the CSRe. In a recent DR experiment of Na-like Kr^{25+} ions at the CSRe, the measured DR rate coefficients were compared with the flexible atomic code (FAC) calculations and AUTOSTRUCTURE code and a very good agreement has been achieved between the experimental results when the strong mixing effects among the low-energy resonances are carefully considered in both calculations.[41]

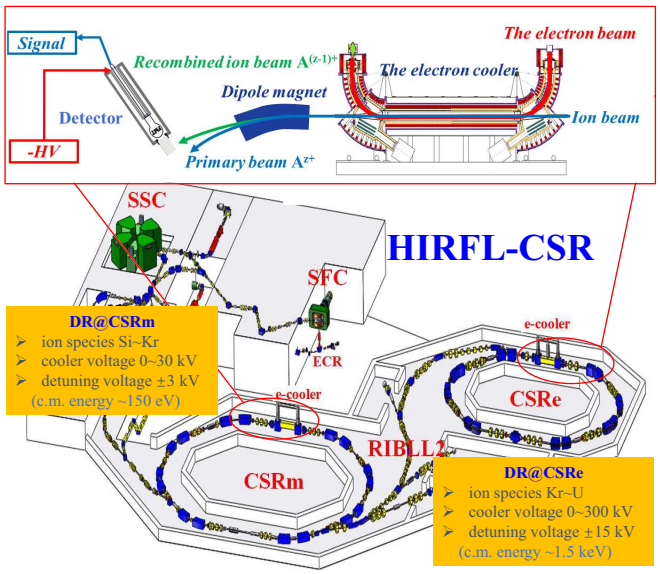


Fig. 3. The layout of DR experiments at the HIRFL facility. The main DR experimental parameters at the CSRm and the CSRe are shown.

Here, we present the DR spectrum of Be-like argon ions[42] as an example. In electron collision with Ar^{14+} ions, the most significant recombination channels in the collision energy range of 0 eV–60 eV are

$$\mathrm{Ar}^{14+}(2s^{2}\,{}^{1}S_0)+e^{-}\rightarrow\begin{cases}\mathrm{Ar}^{13+}[2s^2nl]+h\nu, & \mathrm{RR},\\ \mathrm{Ar}^{13+}[2s2p({}^{3}P_{0,1,2})nl], & n\geq 10,\ \mathrm{DR},\\ \mathrm{Ar}^{13+}[2s2p({}^{1}P_{1})nl], & n\geq 7,\ \mathrm{DR},\\ \mathrm{Ar}^{13+}[2p^2({}^{3}P_{0,1,2};\,{}^{1}D_2;\,{}^{1}S_0)nl], & n\geq 6,\ \mathrm{TR},\end{cases}\quad(1)$$

where RR, DR, and TR denote radiative, dielectronic, and tri-electronic recombinations, respectively. In the case of TR, the capture is associated with the excitation of two core electrons to excited levels and is completed when the triply-excited intermediate level decays by photoemission. The experimental DR spectra of Be-like $^{40}Ar^{14+}$ and theoretical calculations from the AUTOSTRUCTURE code are compared as shown in Fig. 4. The measured spectrum covers the whole energy range of DR resonances associated with $2s \rightarrow 2p$ ($\Delta N = 0$) core excitations. The associated Rydberg resonance series of the doubly excited intermediate levels $2s2p(^1P_1)nl$ and $2s2p(^3P_J)nl$ are indicated by vertical bars with different colors. By fitting the first 13 resonance peaks at relative energy below 0.5 eV with a flattened Maxwellian function,[42] the longitudinal and transversal electron temperatures were obtained, yielding the electron beam longitudinal temperature $k_B T_{\parallel} = 2.40\,(6)$ meV

and transverse temperature $k_B T_\perp = 11.91\,(87)$ meV, respectively. The corresponding experimental energy resolution is better than 0.07-eV full width at half maximum at a relative energy around 0.2 eV. Trielectronic recombination (TR) resonances associated with $2s^2 \rightarrow 2p^2$ core transitions were found surprisingly strongly contributed to the total recombination rate coefficients in the measured energy region.

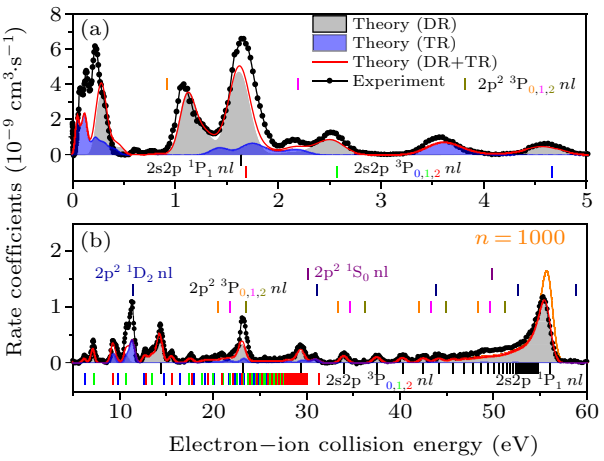


Fig. 4. Electron–ion recombination rate coefficients of Be-like argon as a function of relative collision energy. The orange curve from 45 eV to 60 eV is the theoretical result including the full DR resonance strength up to $n_{max} = 1000$, called the field-ionization-free recombination rate coefficient. Reproduced with permission from Ref. [42].

Progresses related to electron correlation, metastable states, and higher order QED effects have been achieved in the investigation of DR spectroscopy at the storage rings. Some of typical examples will be briefly discussed bellow, trielectronic recombination (TR) resonances associated with $2s^2 \rightarrow 2p^2$ core transitions were not negligible in the resonant spectra and have strong contributions to the total recombination rate coefficients of Be-like Ar^{14+} and Ca^{16+} ions.[39,43] Resonant recombination from parent ions in the long-lived metastable state $2s2p\ ^3P_0$ has been identified in the DR spectrum of Ca^{16+} ions below the collision energy of 1.25 eV, which means the DR measurements of metastable ions can be applied at storage rings.[39] The DR spectrum for the F-like Ni^{19+} ions has been used as a benchmark to evaluate the JAC calculation methods.[44,45] Moreover, the $2s^2 2p^5[^2P_{1/2}] \rightarrow 2s2p^6[^2S_{1/2}]$ core transition energy in the F-like Ni^{19+} ions has been precisely determined and the second order QED effects are tested, which benefits from the accurate measurement of the low-lying dielectronic resonances associated with the $(2s2p^6[^2S_{1/2}]6s)J = 1$ intermediate state and the precise calculations of the binding energy of the 6s Rydberg electrons.[46] In addition, strong mixing effects between the low lying $\Delta n = 0$ and $\Delta n = 1$ DR resonances have been revealed in the investigation of DR spectroscopy for the Na-like Kr^{25+} ions.[41]

In the past few years, a series of DR experiments for different HCIs have been investigated at the CSR, such as $Ar^{12+,13+,14+,15+}$, $Ca^{14+,16+,17+}$, Ni^{19+}, and Kr^{25+} ions, electron correlations are studied.[39,41,42,45,47–49] In addition, a large accelerator facility of High-Intensity heavy-ion Accelerator Facility (HIAF)[50] is being under construction by the Institute of Modern Physics at Huizhou city in Guangdong Province. The DR spectroscopy of highly charged ions by employing an electron cooler and an independent ultra-cold electron target is listed as one of the main scientific goals of HIAF project, the detailed description can be found in Refs. [51,52].

2.2. DR and x-ray/VUV spectroscopy at EBITs

In addition to DR experiments at storage rings, DR spectroscopy has also been carried out at EBITs to investigate HCI structures around the world. Since the first experiment[53] at the Livermore electron beam ion trap (EBIT), many measurements have been conducted for He-like ions, such as argon,[54] titanium,[55] iron,[56] nickel,[53] germanium,[57] krypton,[58] molybdenum,[59] iodine,[60] xenon,[61] barium,[59] tungsten,[62] mercury,[63] and isoelectronic sequences with lower charge state.[61,64] Up to now, only a few measurements for H-like ions, such as argon,[65] titanium,[66] and krypton,[67] have been studied due to the experimental difficulties at EBITs.

Since DR only involves one active bound electron, the measurements of resonance strengths and/or cross-sections pave a pathway towards the collision dynamics. A lot of measurements on DR mainly focused on the DR resonance strengths and cross-sections. For instance, Nakamura *et al.*[68] measured resonance strengths of Li-like iodine, holmium, and bismuth, and it has been shown that the generalized Breit interaction (GBI) strongly affects the resonance strengths, as shown in Fig. 5. Yao *et al.*[61] measured the KLL-DR resonance strengths of He- to O-like xenon ions and found that theoretical results of Li-like Xe are about 14% smaller than the experimental ones. Xiong *et al.*[64] carried out the measurements for Li- to O-like gold and deduced a scaling law for B-like and C-like ions. Apart from the resonance strength studies, the strong quantum interference effect between DR and radiative recombination (RR) is expected and investigated as their amplitudes become comparable in the high-Z region.[69]

Very recently, a large modification by the Breit interaction for electric-dipole (E1)-allowed transitions of inner-shell excited states formed in the DR process of highly charged heavy ions was predicted and demonstrated by Hu *et al.*[70] at the Shanghai-EBIT and the Tokyo-EBIT. The relative transition rates are obtained for two dominant radiative transitions from the $1s2s\ ^2 2p_{1/2} 2p_{3/2}$ inner shell excited state of B-like tungsten and bismuth ions to $1s^2 2s^2 2p_{1/2}$ and $1s^2 2s\ ^2 2p_{3/2}$, and it was found that the transition rate ratio between the two transitions is affected by the retardation effect up to more than 100%, as shown in Fig. 6. It provides a large possibility to test

the first-order QED effect using the DR experiments.[71]

It is interesting to note that higher-order interactions, namely trielectronic and quadruelectronic recombination (TR and QR), significantly contribute to the recombination resonance strength due to the relatively strong configuration mixing effect in medium-heavy ions.[72] Unlike the intra-shell TR process at low collision energy observed in the storage ring,[73] the higher-order processes studied in EBIT involve K–L inter-shell resonance. As pointed out in[74] the higher-order recombination contribution decreases fast with increasing atomic number (Z^{-4}). The inter-shell TR contribution overwhelms the DR in argon ions, while the contribution is below 6% to the total resonant strength in C-like Kr^{30+}.[75] The higher-order interaction could be neglected in heavier ions, while other effects may have large contributions.

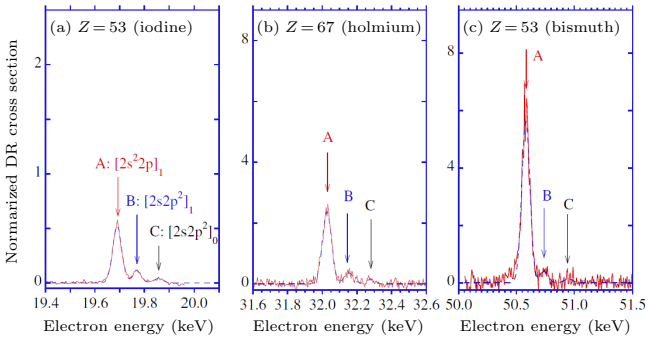


Fig. 5. Dielectronic recombination cross sections for the $KL_{12}L_{12}$ region of Li-like ions normalized to the ionization cross sections of Be-like ions for iodine ($Z = 53$), holmium ($Z = 67$), and bismuth ($Z = 83$). The horizontal energy scale was calibrated with the theoretical resonance energy. The solid red line shows experimental results and the broken blue line of the Gaussian functions are fitted to the experimental data.[68] Reproduced with permission from Ref. [68].

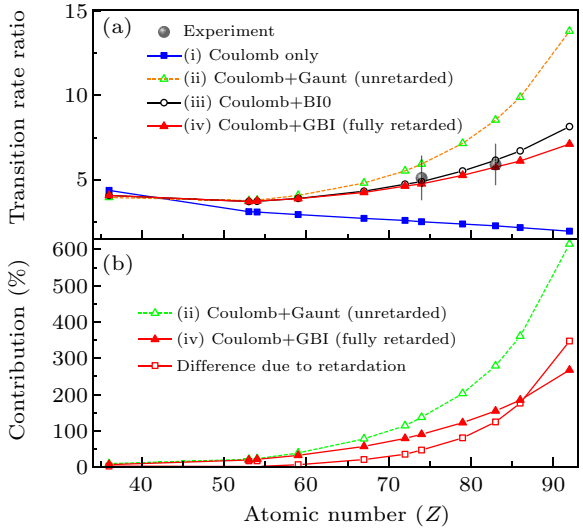


Fig. 6. (a) Transition rate ratio between two radiative transition paths of the $1s2s^22p_{1/2}2p_{3/2}$ inner shell excited state formed in DR. The black circles represent the experimental results.[70] The other four symbols with solid or dashed lines are the results of four sets of calculations. (b) Retardation induced difference (open squares) of the contributions to the radiative transition ratios. Reproduced with permission from Ref. [70].

In EBITs, HCIs are produced by collision ionization with a mono-energetic electron beam and confined in an ion trap with low ion temperature. The spectroscopy of HCIs is usually free of satellite blending and free from Doppler effects compared to the accelerator measurements, therefore high precision measurements of x-ray and VUV radiations can be performed. High-resolution crystal spectrometers are usually used to detect Kα lines in medium-Z ions, *e.g.*, the absolute wavelengths of the w ($1s2p\ ^1P_1 \rightarrow 1s^2\ ^1S_0$) resonance lines in He-like ions are measured in EBITs[76–78] for testing QED effects. One remarkable result was reported by Chantler *et al.*,[76] in which a systematic discrepancy between the experiments of the w line transition energies and the calculations including two-electron QED corrections and a Z^3 dependent divergence were shown. However, the measurements for S^{14+}, Ar^{16+}, and Fe^{24+} ions[77] supported the state-of-the-art bound-state QED calculations. Experimental results on Kr^{34+} measured in EBIT with synchrotron radiation excitation technique also supported the theory.[79] Most of the available experimental results have larger uncertainties than the contributions from the screened vacuum polarization and two-photon exchange corrections. Experiments with improved precision are necessary to test these terms. In the high-Z ions, experiments mostly focused on measuring the energies of the $2p_{3/2} \rightarrow 2p_{1/2}$, $2s_{1/2}$ transitions[80,81] in the x-ray domain, and the $2p_{1/2} \rightarrow 2s_{1/2}$ transitions[82] in the extreme ultraviolet domain. Figure 7 shows the spectrum of the $2p_{1/2} \rightarrow 2s_{1/2}$ transitions in U^{88+} and U^{89+} and its calibration spectrum measured by Beiersdorfer *et al.*[82] The result for U^{89+} established a benchmark for testing QED contribution to the transition energy with an accuracy of 3.6×10^{-4}.[82]

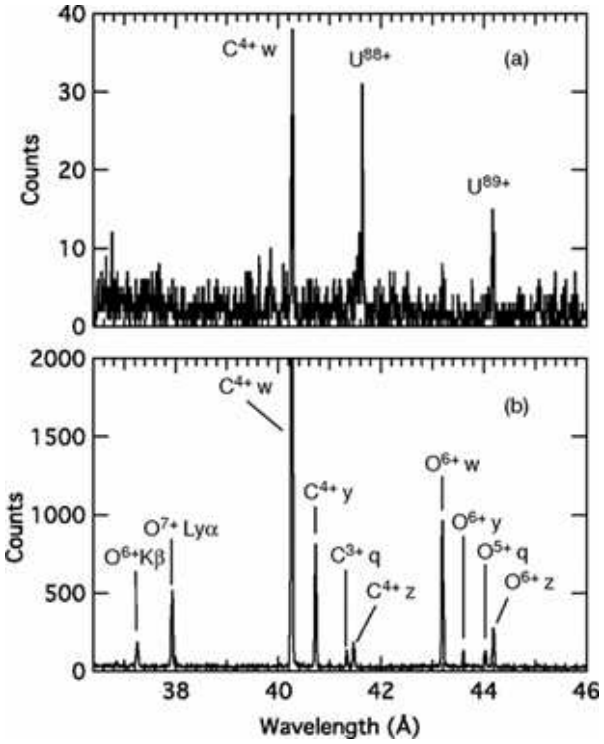


Fig. 7. (a) Spectrum of the $2p_{1/2} \rightarrow 2s_{1/2}$ transition in U^{88+} and U^{89+}. (b) Calibration spectrum. Reproduced with permission from Ref. [82].

Precision spectroscopy of HCIs in EBIT is also applicable to the diagnostic of fusion plasmas and astrophysical plasmas.[83–86] Since the accurate prediction of the atomic structure in complex systems is still a big challenge for theories, benchmark experiments are essentially required. One such example is tungsten, which will be used in future TOKAMAKs. Spectroscopies of highly charged tungsten ions studied in EBITs cover optical,[87] UV,[88,89] and x-rays spectra.[83,86] Figure 8 (adopted from Ref. [83]) shows a high-resolution x-ray spectrum of Cu- and Ni-like tungsten ions measured in Shanghai-EBIT.[90] The experimental wavelength provides important reference data for electron correlation studies in multi-electron ions and is also applied to determine the toroidal rotation velocity of the ions in the TOKAMAK.[83] To diagnose the temperature and density of fusion plasmas,[86,88] intensity ratios of EUV lines from highly charged Ar, Fe, and other ions are measured in EBITs.[84,85] It also provides an opportunity to determine the magnetic field in solar flares or the corona as proposed in Ref. [91].

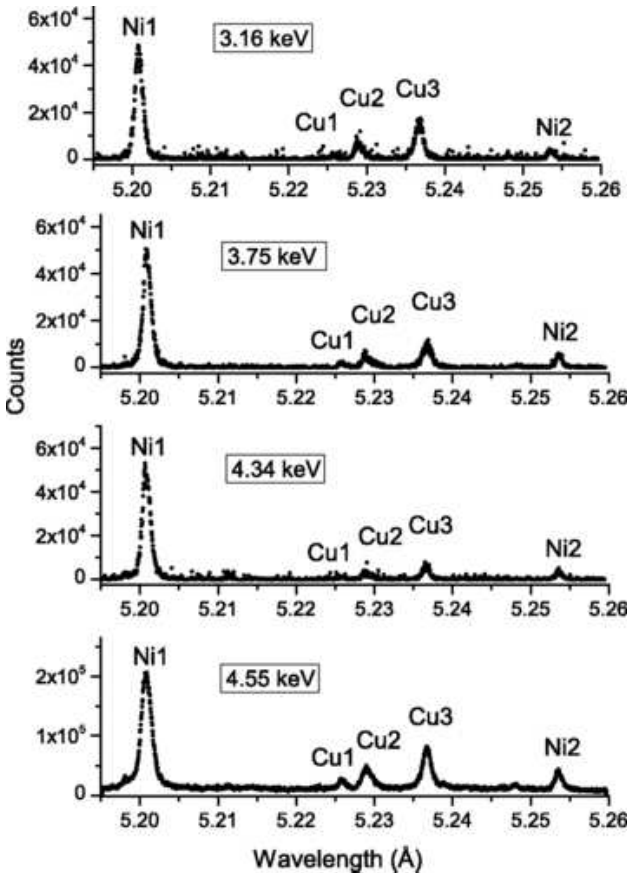


Fig. 8. X-ray spectra of Cu- and Ni-like W ions measured in Shanghai-EBIT. Reproduced with permission from Ref. [83].

Using the beam scanning method, DR processes and the correlated x-ray emission could be studied simultaneously in EBIT. Figure 9 shows a typical three-dimensional spectrum of the DR process of xenon ions in Shanghai-EBIT.[90] The resonance peaks represent the KLL-DR events of He-like to N-like Xe ions. The continuous band is from the radiative recombination (RR) to the L-shell of the corresponding ions. By normalizing DR to the theoretical $n = 2$ RR cross-sections, for which the uncertainty is considered to be about 3%, the DR resonance strength could be determined. The method has been well applied to measure the DR resonance strength that involves an inner-shell electron excitation.[61–64] Many other measurements use a steady-state running mode.[60,92] In this mode, the electron beam energy is slowly scanned to ensure that the charge state distribution (CSD) reaches equilibrium at each beam energy. The resonance strength can be extracted from the ionization equilibrium rate equation by normalizing it to the calculated electron impact ionization cross-sections.[60,92]

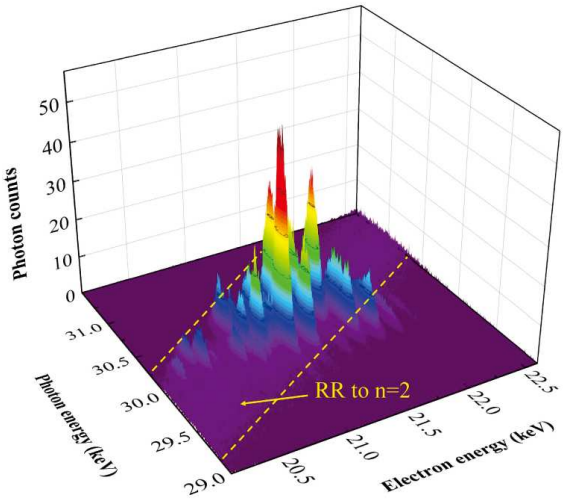


Fig. 9. A typical three-dimensional spectrum of DR measurement in EBIT. The x-ray intensity (Z axis) is a function of the incident electron energy for the X axis and its photon energy for the Y axis.

In the meantime, anisotropy and polarization of DR x-ray emissions have attracted much interest. Breit interaction is, generally, considered a minor correction to the dominant Coulomb repulsion in electron-electron interaction. However, Fritzsche *et al.*[93] predicted that anisotropy of x-ray line emission from DR is dominated by the Breit interaction, which was soon confirmed by Hu *et al.*[94] at the Tokyo-EBIT. Inspired by these seminal works, more efforts have been made to explore this unexpected effect. At the Heidelberg-EBIT, Jörg *et al.*[95] made the first polarization measurement of DR x-ray emissions of Be-like and Li-like xenon ions using Compton polarimetry, which are highly sensitive to the Breit interaction. Shah *et al.*[58] extended these investigations to a lighter element of He-like through O-like krypton ions and also confirmed a high sensitivity to the Breit effect. Amaro *et al.*[96] also studied the angular distribution of DR lines of highly charged krypton ions, they demonstrated that the Breit effect on the anisotropy of DR x-ray emissions is strongly state-selective. Furthermore, the polarization of DR x-rays can be used as an important diagnostics tool for hot plasmas. Shah *et*

al.[97] investigated higher-order resonant contributions to DR x-ray line polarization and claimed that polarization measurement could be a useful approach to diagnose the electron temperature of hot plasmas. In addition, Shah *et al.*[98] claimed that polarization of DR satellite lines could be used in diagnosing anisotropies of hot celestial plasmas.

In addition to the investigation of the QED effect and Breit interaction, HCIs have been proposed to enable sensitive tests of physics beyond the standard model and the realization of high-accuracy atomic clocks, owing to their high sensitivity to fundamental physics and insensitivity to external perturbations.[99] Very recently, the Coulomb crystallization of B-like $^{40}Ar^{13+}$ has been realized in a cryogenic linear radiofrequency trap by means of sympathetic cooling through Coulomb interaction with a directly laser-cooled ensemble of Be^{+} ions.[100] Furthermore, coherent laser spectroscopy of highly charged $^{40}Ar^{13+}$ ions has been achieved using the quantum logic technique, and the determined absolute frequency of the $^{40}Ar^{13+}$ fine-structure transition reached an uncertainty of 3×10^{-15}, which pave the way for future HCI clock investigation and applications.[101] With this strong motivation, the fine structure splitting $1s^22s^22p\ ^2P_{1/2}$–$^2P_{3/2}$ transitions in boron-like S^{11+} and Cl^{12+} was experimentally measured with a high precision spectrometer at the Shanghai High-Temperature Superconducting electron beam ion trap (SH-HtscEBIT). The M1 transition wavelengths for S^{11+} and Cl^{12+} were determined to be 760.9635(29) nm and 574.1539(26) nm (in the air), respectively. The M1 transition energies in S^{11+} and Cl^{12+} were evaluated within the *ab initio* QED framework to compare with the experimental data and provide a possibility to test QED effects and correlation effects with high accuracy in few-electron highly charged ions.[102]

2.3. Test of QED via x-ray spectroscopy in strong electromagnetic fields

Quantum electrodynamics (QED) describes the interaction between light and matter and is by far the most rigorously tested theory in physical science under weak field conditions. The experiments to test the bound-state QED effect are mainly carried out from the following aspects: inner-shell atomic transition energy measurement, direct measurement of bound energy, and measurement of the g-factor of a bound electron. Due to the complicated electron correlation and interaction in multi-electron atomic systems, theoretical calculations are very difficult. Generally, high precision calculations are performed for hydrogen-, helium- and lithium-like systems. Hydrogen atom is the ideal system for studying bound-state QED and great progress has been made in precision measurements in recent decades. The experimental relative accuracy of transition energy is better than 10^{-12},[103,104] the accuracy of ground state Lamb shift measurement reaches a fraction of ppm,[105] which is limited by the uncertainty of proton radius. The experimental g factor is in agreement with theory at the level of 7×10^{-11}.[106] On the whole, the experimental accuracy is higher than that of theoretical calculations for light atomic systems.[1] One has to note, that the success of the QED prediction of the experiment is in weak fields, where perturbation approximation is appropriate. On the other hand, a precise test of QED in a strong electromagnetic field is far from satisfactory. Highly charged heavy ions provide strong electromagnetic field conditions, for example, the 1s electron of hydrogen-like uranium ion experiences a field of about 10^{16} V/cm, which is 10^6 times stronger than that in the hydrogen atom. Under such extreme field conditions, the validity of the perturbation theory that deals with hydrogen atoms accurately should be questioned.[107] Therefore, the test of QED in a strong field attracts great interest in the last decades, and it may also provide important evidence for the search for new physics beyond the standard model.[105,108]

The experimental study of the QED effect in a strong Coulomb field has been greatly advanced with the advent of superEBIT at Livermore[80] and the heavy-ion storage rings ESR in Darmstadt[109] and CSR in Lanzhou.[110] At the same time, theoretical studies of QED of hydrogen-like and few-electron heavy ions made significant progress in the non-perturbative region, from the consideration of first-order self-energy (SE) effect to first-order vacuum polarization (VP), extended to the complete second-order Feynman diagram of SE and VP.[111] Now, theoretical studies on strong-field QED to all orders of αZ[4,111] are available. For heavy ions, the transition energy to K-shell is in the soft to hard x-ray range, and usually, are measured by high purity germanium detectors. Here we give an example of a strong field QED test performed at the electron cooler of ESR using bare uranium U^{92+}. Figure 10 shows the progress in the experimental accuracy of the 1s Lamb shift in hydrogenlike uranium in the last 30 years. The accuracy has been improved from 429 ± 63 eV ($\Delta E/E=15\%$) in the 1990s to 460.2 ± 4.6 eV ($\Delta E/E\approx1\%$) in 2005, the highest accuracy available to date in the strongest field.[112] Since then there is no breakthrough in the 1s state Lamb shift measurements for H-like uranium due to the lack of significant advances in experimental methods and the unavoidable strong Doppler effect of fast moving ions. Although big efforts have been made to improve the accuracy, such as crystal spectrometer FOCAL.[113] and microcalorimeter,[114] the achieved accuracy is far from satisfactory for H-like gold ions.

However, the measurements of the Li-like heavy-ion system are making excellent advances in recent years, especially in the EBIT experiments. The reason is that the transition energy of the $2p_{1/2}$, $2p_{3/2}$–$2s_{1/2}$ is well in the detection range of the advanced microcalorimeter and traditional crystal

spectrometer, and high accuracy data were available.[116,117] Beiersdorfer *et al.* inferred a value for 2s two-loop Lamb shift in U^{89+} of -0.23 eV through the SuperEBIT measurement.[82] Bruhns *et al.* used Heidelberg EBIT and x-ray spectrometer and reported the experimental uncertainty for the Lyman-α_1 wavelength of Cl^{16+} which is reduced by a factor of 3.[4,118] As pointed out by Beiersdorfer in a recent review,[116] the transition energy measurements of high-Z lithium-like ions are ready to test two-loop QED at a level similar to that achieved with atomic hydrogen. The main factor limiting the uncertainties in present measurements to test two-loop QED is the finite size of nuclei. In the meantime, both experimental and theoretical studies on He-like systems are making progress and the experimental determination of the hyperfine structure in an H-like heavy system is ahead of theoretical accuracy.[119] Therefore, this field of testing QED in strong electromagnetic fields has also not yet reached its ultimate potential and there may be possible surprises in the future.

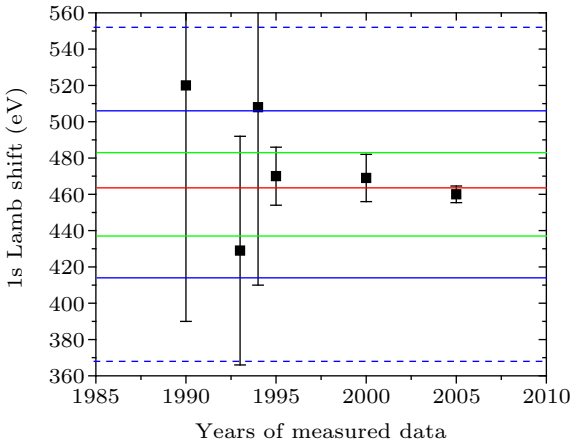


Fig. 10. Ground state QED measurements of H-like uranium U^{91+} at ESR storage ring at GSI. The red line is the latest theoretical value QED calculations performed to all orders in the parameter $Z\alpha$, where α is the fine structure constant.[115]

2.4. Applications in the astrophysical and fusion plasmas

Cosmic plasmas can be divided into two broad classes depending on the different temperatures: electron-ionized and photoionized. Electron-ionized plasmas are formed in stellar atmospheres, supernova remnants, the interstellar medium, galaxies, and clusters of galaxies. Photoionized plasmas are formed in the environments of planetary nebulae, the intergalactic medium, x-ray binaries, and active galactic nuclei. Spectroscopic observations of the plasmas have been used to infer the properties of the cosmos. To reliably interpret the observed spectra from photoionized and electron-ionized plasmas, an accurate understanding of the ionization balance of the source is essentially required. Of particular importance are the accurate rate coefficients for electron impact ionization (EII) and DR processes. The situation is very similar for the fusion plasmas, and the accurate DR rate coefficients for tungsten ions and other impurities like argon, krypton, xeon, *etc.* in different charge states are essential to build up the ionization balance and to diagnose the status and key parameters. However, at present, most of the data used in plasma modeling codes were produced by theoretical calculations. To assess the reliability of these calculations benchmarking experiments are vitally needed. In the past decade, a series of DR measurements of astrophysical relevant HCIs has been peformed by employing the electron-ion merged-beams technique at the cooler storage ring CSRm and CSRe at the Institute of Modern Physics, Chinese Academy of Sciences. In particular, Li-, Be-, B-, and C-like argon and calcium ions have been systematically investigated.[39,42,47–49,120] Iron ions are the most abundant heavy elements in the universe and the ions with different charge states are of special interests to astrophysical plasma studies, therefore, corresponding experimental work on DR of $Fe^{(7-14)+}$ and $Fe^{(18-22)+}$ ions has been carried out at the storage ring TSR over already more than one decade. The experimental data resulting from this effort are summarized and has been published in Ref. [121], and these experimental benchmarks are thus indispensable for arriving at a reliable DR data base for the astrophysical modeling, particularly, of low-temperature plasmas.[122] Tungsten ($Z = 74$) is assumed to be the plasma-facing component in the international tokamak reactor, International Thermonuclear Experimental Reactor (ITER), because of its thermo-mechanical properties, such as high melting point, low sputtering yield and low tritium retention rates.[123] As a result, tungsten ions received much attention from the magnetic confinement fusion community. The accurate data of the electron–ion recombination processes of tungsten ions, such as DR and RR, are very important to understand the properties of the fusion plasmas. In an effort to provide a sound experimental basis for calculations of the recombination rate coefficients of open f-shell tungsten ions, a series of DR measurements of tungsten ions W^{18+}, W^{19+}, W^{20+}, and W^{21+} have been conducted at the heavy ion storage ring TSR at MPIK in Heidelberg.[124] In addition, a systematic theoretical calculations of recombination rate coefficients for tungsten ions have been performed by employing the AUTOSTRUCTURE code and can be found in the references in Refs. [125–127].

In contrast to the very narrow velocity spread of the electron beam in a storage ring experiment, the electrons in the astrophysical and fusion plasmas have a much broader and isotropic Maxwellian velocity spread. Therefore, temperature-dependent plasma recombination rate coefficients (PRRC) can be obtained through the convolution of the DR cross-section $\sigma(E)$ and a Maxwell–Boltzmann distribution characterized by the plasma electron temperature T_e as shown below:

$$\alpha(T_e) = \int \alpha(E) f(E, T_e)\, \mathrm{d}E, \tag{2}$$

where $f(E,T_e)$ is the electron energy distribution function, which can be expressed as

$$f(E,T_e)=\frac{2E^{1/2}}{\pi^{1/2}(kT_e)^{3/2}}\exp\left(-\frac{E}{kT_e}\right). \quad (3)$$

In the following discussion, the Be-like Ar^{14+} ions are used as an example. The experimentally derived and theoretically calculated plasma rate coefficients as a function of electron temperature are shown in Fig. 11 with the solid red line and the short-dashed red line,[42] respectively. Similarly, the theoretically calculated DR and TR contributions are shown in Fig. 11 with the black dashed line and the blue dot-dashed line, respectively. The temperatures range from 10^3 K to 10^7 K, which includes the ranges of photoionized and collisionally ionized plasmas for Be-like Ar^{14+}. The boundaries of these temperature ranges are displayed by vertical dashed lines. At a temperature of 10^3 K, the TR contribution is dominant and a factor of four larger than the DR contribution. In the temperature range of photoionized plasmas, the TR contribution to the total plasma rate coefficient amounts to 10%. The experimentally derived plasma rate coefficients are 60% larger and 30% lower than the previously recommended atomic data for the temperature ranges of photoionized plasmas and collision-ionized plasmas, respectively. However, good agreement was found between experimental results and the calculations by Gu *et al.*[128] and Colgan *et al.*[129] The present results constitute a set of benchmark data that can be used in astrophysical and fusion plasma modeling.

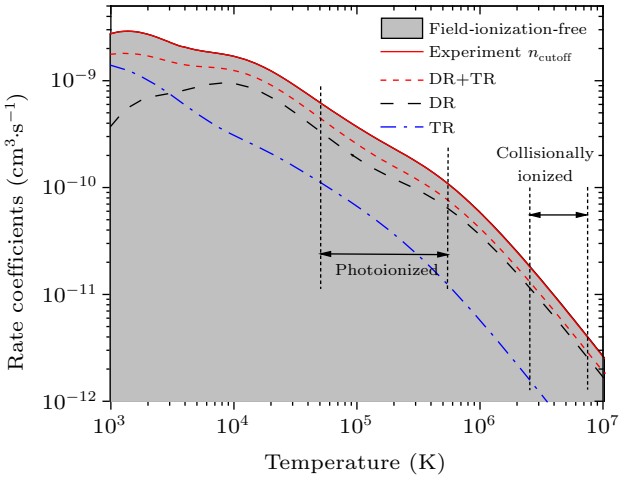


Fig. 11. Plasma rate coefficients of Be-like Ar^{14+} as a function of the electron temperature. The solid red line is the experimentally-derived $\Delta N=0$ DR and TR rate coefficients.[42] The theoretical results deduced from the AUTOSTRUCTURE code for $\Delta N=0$ DR and TR are shown as a dotted black line and a dash-dotted blue line, respectively. The calculated sum of DR and TR is shown as a short-dashed red line. The experimentally-derived field-ionization-free plasma rate coefficient is shown as a gray area. Reproduced with permission from Ref. [42].

In order to facilitate the use of experimental DR data in astrophysics and fusion physics modeling, the experimentally-derived plasma rate coefficients are usually parameterized. The fitting function we have used is displayed below:

$$\alpha(T_e)=T_e^{-3/2}\sum_i^n c_i\cdot\exp\left(-\frac{E_i}{kT_e}\right), \quad (4)$$

The fitting parameters of c_i and E_i are listed in Table 1 and reproduce the data within 2% at $\sim 10^3$ K and better than 1% up to 10^7 K.

Table 1. Fitted coefficients for the RR-subtracted $\Delta N=0$ DR + TR rate coefficients for two different values of n_{cutoff} and $n_{max}=1000$ (field-ionization free). The units of c_i and E_i are 10^{-3} cm^3·s^{-1}·K$^{3/2}$ and eV, respectively.

No.	n_{cutoff}		$n_{max}=1000$	
i	c_i	E_i	c_i	E_i
1	0.254	0.12	0.244	0.115
2	0.580	0.28	0.590	0.278
3	3.74	3.47	3.77	3.45
4	5.17	1.43	5.14	1.43
5	14.3	12.42	14.38	12.45
6	23.39	31.84	23.13	31.95
7	38.84	56.39	40.30	57.03

3. Collision dynamics in charge exchange processes

Starting from the end of last century, the invention of many-particle imaging and projection techniques, the so-called reaction microscope, or cold target recoil ion momentum spectroscopy (COLTRIMS) has significantly advanced our abilities in obtaining the full kinematic information of dynamic processes involving the many-body system.[6,7] The first full version of the reaction microscope was developed in studies of ion–atom collision physics.[7] Since then studies of fundamental processes such as the single ionization and single capture have brought us abundant knowledge about few-body quantum dynamics. It should be mentioned that, starting from 2001, the first project of reaction microscope at Lanzhou (ReMiLa) in China was initiated at the Institute of Modern Physics (IMP) and its longitudinal recoil ion momentum resolution reached 0.35 a.u.[130] Figure 12 shows one of typical reaction microscopes implemented on the accelerator.

Nowadays, a series of reaction microscopes have been established at IMP and are specially designed to serve different research goals. For instance, the ReMiLa dedicated to relativistic energy collision has a transversal geometry with respect to the beam line to collect the transversally ejected electrons efficiently. This recoil ion spectrometer has a momentum resolution down to 0.2 a.u. The ReMiLa for collisions in near Bohr velocity region has a geometry of longitudinal spectrum arm and a resolution much better than 0.1 a.u. has been achieved. Recently, the ReMiLa designed for studies on non-charge transfer processes of ion induced excitation has achieved the resolution of 0.45 a.u. Significant progresses in low energy collision have been made.

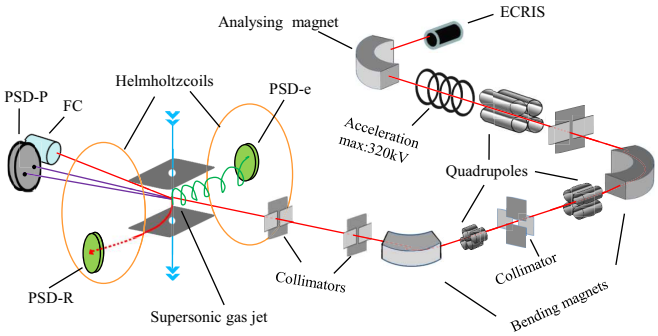


Fig. 12. An overview of the experimental setup at the platform for atomic physics with highly charged ions. PSD represents the microchannel plate position sensitive detector (the suffixes -R, -e, and -P corresponding to recoil ion, electron, and projectile detectors), and FC represents the Faraday cup. Reproduced with permission from Ref. [133].

In beginning of 2000s, a new generation of spectrometers employing magneto optically trapped-target have been developed by incorporating the laser cooling techniques into traditional COLTIMS.[131] Lee *et al.*[132] reported on state-selective capture measurements for 6-keV Cs^+ colliding with rubidium in 5s and 5p states, with a so far unprecedented recoil ion resolution of 0.03 a.u. However, the work is limited by the target species that can be cooled by available laser systems.

In the following subsections, the special attention will be paid on important progresses related to experimental results and comparisons with theoretical results achieved in the past two decades.

3.1. Charge exchange dynamics in slow ion–atom collisions

One of the most important processes in collisions between HCIs and atoms or molecules at low velocity is the electron capture (or charge exchange), which has been the subject of numerous investigations for more than fifty years. In the past two decades, a resurgent interest in this fundamental process arose due to the breakthroughs in experimental techniques and theoretical treatments (see Subsection 3.2). In particular, the studies on the collision dynamics have been fostered by the prevailing application of the reaction microscope technique,[6,7] which enables one to perform, with high efficiency and accuracy, kinematically complete experiments for state-selective electron capture processes and provides rigorous tests of the most sophisticated theories developed up to date. In recent years the increasing demand for the charge exchange data in the associated fields, such as astrophysical observation and ion-induced radiation damage to biological tissues, also significantly motivates relevant studies.

Using the COLTRIMS technique, both the Q-value and projectile scattering angle for single-electron capture (SEC) can be obtained with high precision. The electron capture to the excited states of hydrogen could be distinguished, for the first time, in fast proton on He collisions at the Tandem accelerator of the University of Frankfurt in the late 1990s.[134] Following this pioneering work, numerous studies on state selective cross sections have been performed in different colliding systems, for example, $Ar^{16+} + He$,[135] $Ne^{10+} + He$,[136] $p + He$,[137,138] and $He^{1,2+} + He$.[138,139] In the early stages of such kind studies, only the principal quantum number n, labeling the state the active electron is captured to, can be resolved.

In the following years, better resolution on the recoil ion momentum was achieved by means of dedicated recoil-ion spectrometer and target preparation, which dramatically advance the charge exchange studies towards a more detailed level. For example, an unprecedented momentum resolution for He^+ recoil ion was demonstrated by the Frankfurt group using the so-called time and space-focusing geometry in 2012.[140] With the spectrometer, Kim *et al.*[140] was able to separate the pure transfer process from additional excitation contributions in fast proton–helium collisions. However, the spectrometer was limited to study the system with very low momentum exchange in ion–atom collisions due to its geometry. Later, Fischer *et al.*,[141] developed a longitudinal COLTRIMS and its recoil-momentum resolution is 0.07 a.u., which was limited only by the residual thermal spread of the gas-jet target.[7] With this development, the measurement of the state-selective cross sections with respect to the principal quantum number, subshell level, and even spin state of the captured electron could be accessed. Figure 13 shows the Q-value spectrum and energy levels following single-electron capture in $Ne^{7,8+}$+He collisions at 63 keV. This pioneering work demonstrated that, with recoil ion resolution better than 0.1 a.u., reaction microscope/COLTRIMS can be used to obtain spectroscopic information about energy levels of highly charged ions in electron capture collisions with helium that are not directly accessible by other methods.

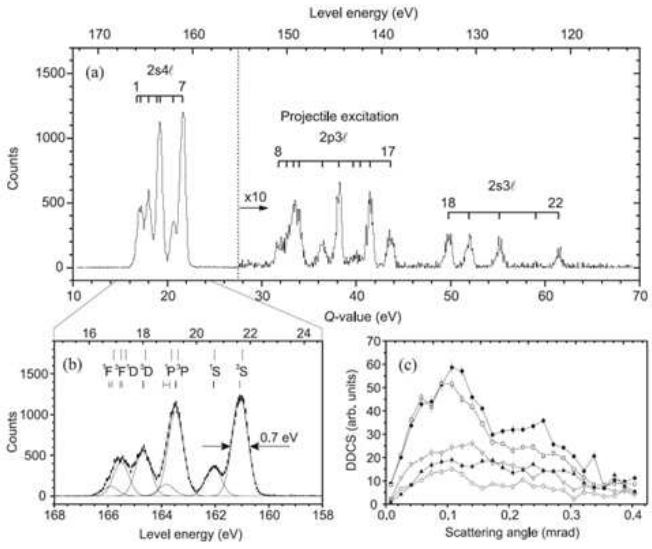


Fig. 13. (a) Q-value spectrum and energy levels of Ne^{6+} following single-electron capture from He at 63 keV. (b) Decomposition of the 2s4l spectrum into different subshells and spin states. (c) Angular differential capture cross sections for the 2s4l states. Reproduced with permission from Ref. [141].

As pointed out in the above paragraphs, the (n,l) distribution of captured electron in the ions can be extracted from the Q-value in collisions of ions and atoms/molecules, which is of important applications in many relevant fields. In the past two decades, the demand of experimental data from astrophysical field considerably promotes the state-selective capture studies. For example, it has been accepted that charge exchange (CX) between solar wind ions, like $O^{7,8+}$, $N^{6,7+}$, $C^{5,6+}$, $Ne^{8,9,10+}$, *etc.* and neutral gas in the interstellar medium contributes significantly to diffuse soft x-ray background. The interpretation of the astronomical observations relies on a large number of laboratory measurements. The access to HCIs provides favorable conditions for laboratory CX studies associated with the modeling of the charge exchange induced x-ray emissions. Beiersdorfer *et al.*[142] simulated the x-ray spectrum from the Comet C/1994 S4, based on the measured x-ray emissions following CX between bare and H-like C, N, O ions and CO_2 at few tens of eV/u at EBIT, and deduced the relative abundance of the solar wind ions. Xu *et al.*[143] reported the n-resolved state selective capture cross sections in a series of new measurements on the charge exchange of $Ne^{(8,9)+}$ ions with He and H_2 for collision energy ranging from 1 keV/u to 24.75 keV/u using COLTRIMS. By applying l distributions commonly used in the astrophysical literature to the measured n-resolved cross sections and considering the radiative cascades from the excited states of Ne^{7+} ions, the soft x-ray emissions in the charge exchange between 4 keV/u Ne^{8+} and He were deduced and compared to the recent x-ray emissions measurement reported by Zhang *et al.*,[144] which provide the first and direct test of the validity of different l distribution models, as shown in Fig. 14. Recently, a new experimental setup for measuring the absolute electron capture cross sections has been equipped at Fudan University. And the cross sections of the single and double charge exchange between the highly charged ion O^{6+} and CO_2, CH_4, H_2, and N_2 were reported.[145] In astrophysics modelling, the atomic data used for CX interpretation are from the database of SPEX,[146] XSPEC,[147] AtomDBCX,[148] *etc.*, where, in most cases, theoretical data are collected but few are verified by experiments. Therefore, CX data from laboratory measurements are strongly required, not only for providing reliable atomic data for modelling astrophysical charge exchange plasma, but also for stringent test of CX collision dynamics.

In addition to Q-value measurement, with COLTRIMS the fully differential cross sections (FDCS) for SEC can also be obtained, which is essential for understanding the underlying reactions mechanism. A large number of investigations on the projectile scattering angle distributions have thus been carried out both experimentally and theoretically. On the theoretical side, different theories such as the refined CTMC method,[149] the Born distorted wave (BDW-4B) approximation,[150] the continuum distorted wave-eikonal initial state (CDW-EIS II) approximation,[151] the two-center basis generator method (TC-BGM),[152] the boundary-corrected first Born approximation,[153] the close coupling methods,[154] *etc.* have been developed. On the experimental side, the FDCSs for SEC have been measured for a large number of collision systems at the n or even (n,l) level, which provides the most stringent test of the theories.

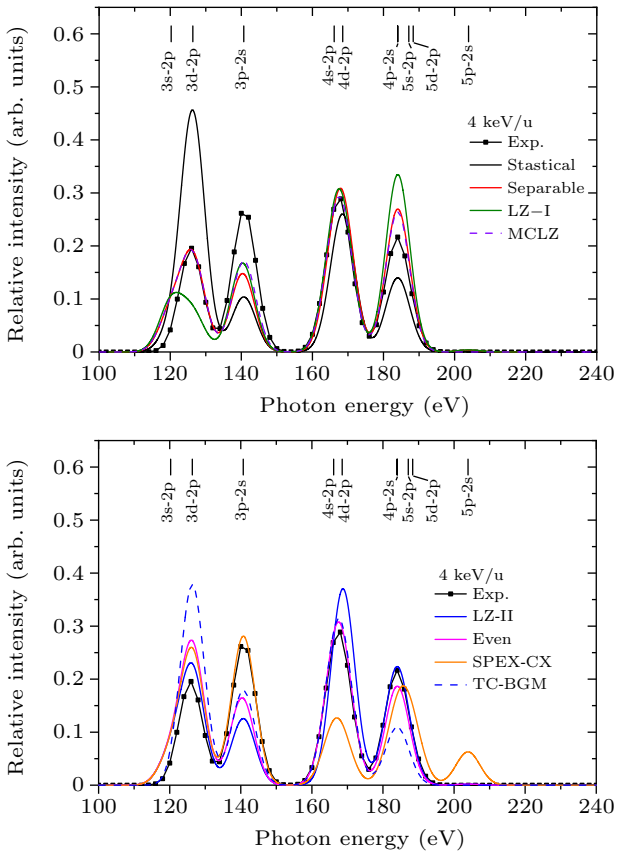


Fig. 14. The normalized emission spectra of Ne^{7+} following CX between 4-keV/u Ne^{8+} and He. Models: statistical (black line), separable (red line), Landau–Zener I (LZ-I) (green line), and even (magenta line). Calculations: MCLZ (purple line), TC-BGM (blue line), and SPEX-CX (orange line). Experiment: Zhang *et al.*[144] (black filled squares). Reproduced with permission from Ref. [143].

Among the various theoretical approaches of different degrees of sophistication, the close coupling methods, such as atomic-orbital close-coupling (AOCC) and molecular-orbital close-coupling (MOCC), have been shown to best describe the experimental results.[18,155,156] For example, in the study of SEC in 3-keV/u Ar^{8+}+He collisions by Zhang *et al.*,[157] it is found the AOCC method can give a reasonable description to n and l resolved cross sections. It is further suggested that 1s to 4s and 1s to 4p state-selective capture processes are mainly caused by radial and rotational coupling effects, respectively, and the $4p_{\pm1}$ quantum states are preferred. Recently, a combined experimental and theoretical study on the SEC in 15 keV/u–50 keV/u C^{4+} + He collisions demonstrates that, in l-resolved angular differential cross sections, an excellent agreement between experimental data and the theoreti-

cal calculations based on the two-active-electron semiclassical AOCC (SCAOCC) method can be achieved[155] as shown in Fig. 15.

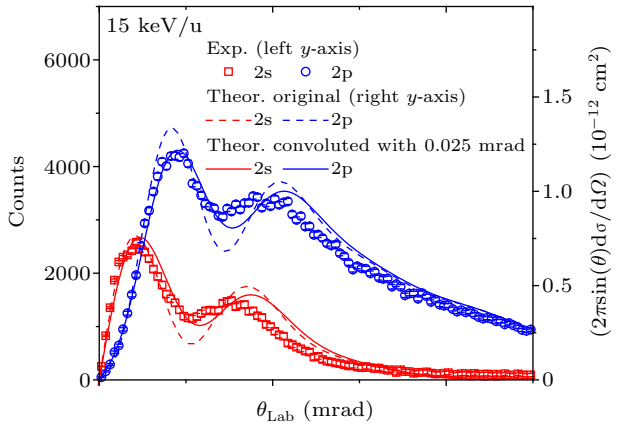


Fig. 15. Angular differential cross sections for capture into 2s and 2p states as a function of $\theta_{\rm LAB}$, scattering angle in the laboratory frame, for C^{4+} + He collisions at 15-keV/u impact energy. Empty symbols: experimental data; dashed lines: SCAOCC results; solid lines: SCAOCC results convoluted with the experimental angular resolution. Reproduced with permission from Ref. [155].

Structures in the angular differential cross sections contain rich information about the collision dynamics. In general, in the small scattering angle regime the nuclear–electron (N–e) interaction is dominant, while the nuclear–nuclear (N–N) interaction mainly governs the large-angle scatterings. However, the origin of the oscillation structure in the scattering angular distributions is still under debate in spite of the numerous studies over the last 40 years. Different mechanisms have been invoked to interpret the structures, such as Stueckelberg oscillation derived from interference between two different reaction paths leading to the same scattering angle,[158] rainbow scattering,[159] interference between the gerade and ungerade scattering amplitudes,[160] the Thomas mechanism due to the kinematical effects,[161] and the Fraunhofer-type diffraction of the matter wave of the projectile.[162] Although usually several of these mechanisms come into play together, it has been widely accepted that the Thomas mechanism is important in the high energy range, meanwhile the Stueckelberg oscillation and molecular states interference are important at low energies.

It is noteworthy that these mechanisms lead to characteristic angular distributions. For example, the Thomas mechanism could lead to a maximum at the characteristic scattering angle of 0.45 mrad for e–e and 0.47 mrad for N–e Thomas process in p + He collisions.[140] Fischer *et al*. concluded that the prominent peak appeared at the scattering angle of 0.47 mrad stemmed from the N–e Thomas mechanisms[163] in the SEC of p + He collisions for energies in the range of 1.3 MeV–12.5 MeV. In the study of slow C^{4+} + He collisions, by adopting Stueckelberg mechanisms into calculations, the peaks at very large angles were nicely reproduced.[164] Note that the studies were focused on large scattering angles partly due to the limited momentum resolution.

Later on, when the improvement of momentum resolution allows one to scrutinize the extremely small angle structure on the order of 10^{-5} rad, the oscillation structure observed in small angle region was found consisting with the Fraunhofer-type diffraction of the de Broglie matter wave of the projectile.[162] as seen in Fig. 16. Van der Poel *et al.* made the first estimation of the oscillating structures in the scattering angle spectra by proposing that the radius of the aperture for Fraunhofer-type diffraction is corresponding to the distance where the single electron capture may take place. Following this work, the Fraunhofer type diffraction in SEC has been revealed in various collision system over a wide impact energy range. The characterization of the radius of the aperture can be generated from different approaches such as the non-perturbative semiclassical approach in combination with Eikonal approximation,[165] CTMC[166] and MCBM.[159] In recent years, further development of the charge exchange theoretical models, for example, the two-active-electron semiclassical atomic-orbital close-coupling (SCAOCC) method,[18,155] provide favorable condition for the investigation into the angular oscillation behavior. For SEC in 15 keV/u–50 keV/u C^{4+} + He collisions, on the basis of the fairly good agreement between the measurements and SCAOCC calculations for both state-selective and angular differential cross sections, further simulations, using an extended Fraunhofer-type diffraction model and the impact parameter dependent transfer probability distribution calculated by SCAOCC method, were performed, which suggest that the oscillation structures observed at small scattering angles for capture to $C^{3+}(1s^22s)$ and $C^{3+}(1s^22p_0)$ can be interpreted as the diffraction pattern of the de Broglie wave of the incident projectile.[155] Considerable efforts from both the experimental and theoretical aspects have been devoted to the understanding of the structure of FDCS by considering subtle correlation effects in different theories. It is now generally accepted that in many cases contributions of the static and the dynamic electron-electron correlation are not negligible in the SEC process.[18,137]

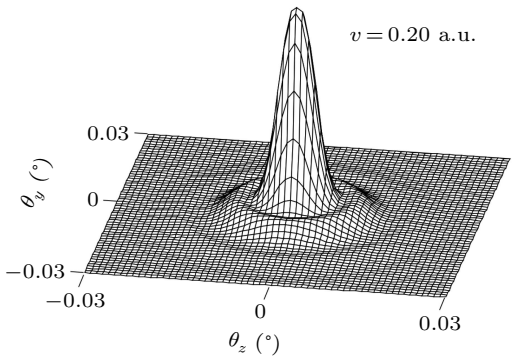


Fig. 16. Angular scattering pattern $\sigma(\theta)$ in 6-keV Li^+ + Na electron transfer collisions. The ring pattern of Fraunhofer-type diffractions is clearly obtained. Reproduced with permission from Ref. [162].

3.2. Recent theoretical progresses in AOCC approach for low energy collisions

In ion–atom collisions, a large number of inelastic processes, such as electron capture or charge transfer, excitation, and ionization, are likely to occur, while the relative strength of the different processes depends strongly on the impact energy.[167] In general, charge transfer dominates at low energies while excitation and ionization take over at large ones. In between, the cross sections for the three types of processes have the largest values and are of comparable importance, the processes are strongly coupled and cannot be described independently to each other. Therefore, the close-coupling approach is readily established as the standard method. Ever since the pioneering work of Ferguson[168] and McCarroll,[169] the electronic wavefunction has been expanded in molecular orbitals or atomic orbitals for describing transitions during collisions. The molecular-orbital close-coupling method (MOCC) is broadly and efficiently applied for low energy collisions, it assumes that the relative velocity of the heavy particles is slow enough that the scattering system can be considered as a quasi-molecule, and coupled molecular orbitals are employed.[170–172] We will not discuss such MOCC here, a review of these methods can be found in Ref. [171] The atomic-orbital close-coupling (AOCC) treatment which is based on the expansion of the scattering wave function onto states of the isolated collision partners and are therefore more suitable for intermediate impact energies. The treatment is semiclassical in that the relative target-projectile motion is described by classical straight-line constant velocity trajectories, while the electronic dynamics is treated quantum mechanically, by solving non-perturbatively the time-dependent Schrödinger equation.[18,173,174] Here the focus will be on the recent theoretical progresses in AOCC approach.

With substantial efforts to understand and model ion–atom collisions over a long period of time,[172,175] one can state that inelastic electronic processes involving only a single electron, such as $H^+ + H$,[176,177] or $He^{2+} + H$ collisions,[178–181] are fairly well understood, while our knowledge on multi-electron ones is still far from complete. A striking example is the double electron capture (DEC) process in $H^+ + H^-$ collisions, which has been extensively investigated for more than five decades.[182–188] Despite its apparent simplicity, a complete theoretical description of the electronic dynamics of this system has only recently been achieved using a fully correlated two-active-electron semiclassical atomic-orbital close-coupling (2eAOCC) method.[154] Figure 17 shows the DEC cross section obtained from 2eAOCC calculations in comparison with available theoretical and experimental results. The 2eAOCC calculations[154] are the first ones to reproduce well the experimental data[182,183,186] in both magnitude and shape, while all previous calculations failed.[182,184,185,188] From the comparisons, one can elucidate that the main differences between the 2eAOCC approach and previous theoretical methods are, (i) the use of much larger basis sets, (ii) the full treatment of electronic correlation, and (iii) the inclusion of pseudostates which span approximately the electron continuum.[154] Taking into account these important ingredients in the theoretical treatment is essential to reproduce quantitatively the DEC cross sections.

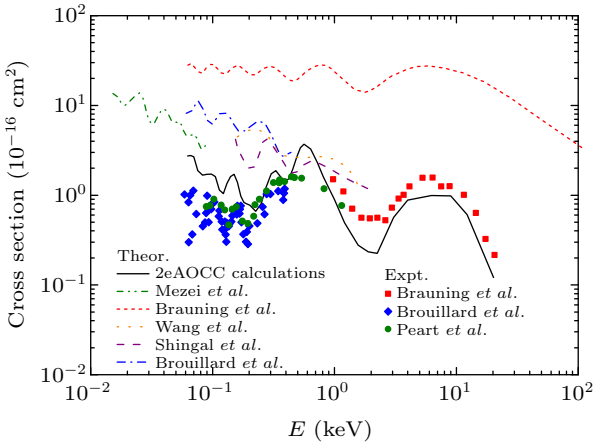


Fig. 17. Double electron capture cross sections in $H^+ + H^-$ collisions: comparison between 2eAOCC calculations[154] and previous experimental and theoretical works. References to indicated previous works are given in Ref. [154]. Reproduced with permission from Ref. [154].

Besides the simplest two-electron system, the 2eAOCC approach has also been applied to the study of multiply charged projectile and helium collisions. As a typical study, figure 18 shows cross sections of SEC and DEC in $C^{4+} + He$ collisions.[18] It can be seen that the results of 2eAOCC calculations and quantum-mechanical molecular-orbital close-coupling calculations join each other smoothly at around 1 keV/u, showing very good agreements[189] with available measurements. In particular, for higher impact energies up to 50 keV/u the state-selective SEC cross sections from 2eAOCC calculations have been confirmed by recent measurements using COLTRIMS.[155]

Recently, the AOCC approach has also been successfully extended to treat three-electron system,[174] we present here an example in Fig. 19: the angular-differential cross section for electron capture from the target ground state to the projectile ground state in $He^+ + He$ collisions at 60 keV/u.[174] Note that the angular-differential cross section allows the analysis of the spatial selectivity of electronic processes, which provides a more stringent test of the theoretical treatment. It can be seen from Fig. 19 that the fully correlated three-electron AOCC calculations (that uses the eikonal approximation to extract the angular-differential cross section.[172,190]) reproduce very well the experimental data,[139] while not for the results from previous perturbative methods.[139,191]

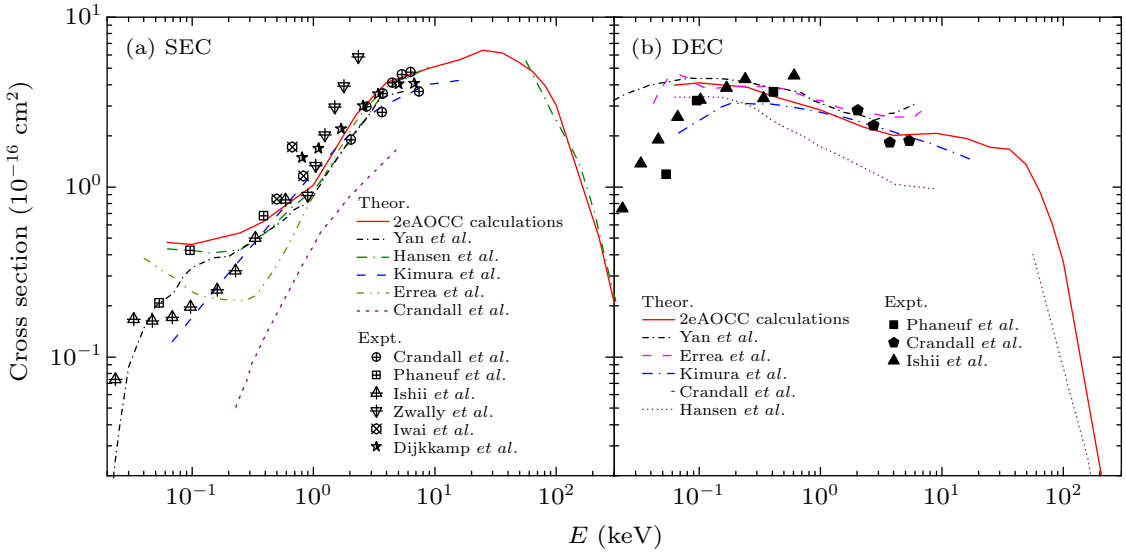


Fig. 18. SEC and DEC cross sections for C^{4+} + He collisions: comparison between 2eAOCC calculations[18] and previous experimental and theoretical works. References to indicated previous works are given in Ref. [18]. Reproduced with permission from Ref. [18].

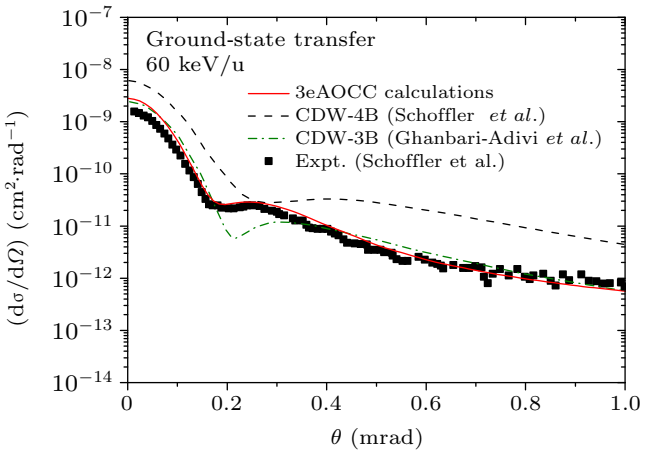


Fig. 19. Angular differential cross sections for ground-state transfer in He^+ + He collisions at 60 keV/u as a function of scattering angle. References to indicated previous results are given in Ref. [174]. Reproduced with permission from Ref. [174].

To date, thanks to the advances in N-active-electron ($N \geq 2$) close-coupling approach we have reached a very good quality of the description of electronic processes occurring in the few-electron collision system at intermediate energies. However, bigger challenges still remain in the treatment of many-electron systems of relevance for applications. In particular, inelastic processes in ion–atom collisions play a central role in many applications going from hadron-therapy to fusion plasma and astrophysics.[192–196] Accurate cross sections are crucial input data of more macroscopic models. For example, the collision between ions and water molecules, since the latter represents 70% (in mass) of the human body and is one of the most abundant species in the universe, the understanding of the fundamental mechanisms occurring in collisions of ions and water molecules is therefore of significant importance in radiobiology and astrophysics. However, to our knowledge, there is no complete close-coupling calculations for such kind of systems, where both electronic correlations and the multi-center character of molecular targets should be taken into account.

3.3. Many-body dynamics at high collision energies

The most fundamental and interesting processes in atomic collision physics occur already at nonrelativistic collisions of bare projectile ions with atomic/molecular targets. Additional processes can occur when the relative velocity of colliding systems approaches the speed of light, such as electron–positron pair production which dominates any other production of matter and anti-matter pairs. The investigations of all these processes in relativistic collisions have attracted much attention in the literature (see Refs. [197–201]).

Besides, the electromagnetic interaction between colliding partners in relativistic collisions is more complicated, a detailed description of relativistic collisions involving three or more active particles, represents a strong challenge for theory, and many phenomena occurring in such collisions are less understood compared to their non-relativistic counterparts. Therefore, studies of collisions involving relativistic charged projectiles with atoms/molecules allow one to obtain valuable information about the modifications of physical processes occurring due to relativistic effects, and also to get a better insight into the non-relativistic collision physics.

Furthermore, the ionization of atoms/molecules by charged projectiles is of fundamental importance for a detailed understanding of the matter response to the action of electromagnetic fields. For instance, the ionization of an atomic/molecular system by charged particles and due to the photoeffect are very closely connected if the former ionization caused by charged particle involves exchange of a virtual photon with a ‘strong’ transverse and a ‘weak’ longitudinal

component, especially if the energy–momentum properties of such a virtual photon would also be very close to those of a real photon. Thus, the fundamental similarity between ionization of an atomic/molecular system due to the photoeffect and charged particle can be observed only in the domain of relativistic collisions provided $\omega/v_p\gamma \ll |q_{tr}| \ll \omega/v_p$. With ω being the transition energy in the target, v_p the collision velocity, q_{tr} is transverse momentum transferred during the collision to the target, $\gamma = (1-v_p^2/c^2)^{-1/2}$ is the Lorentz factor and c the speed of light.

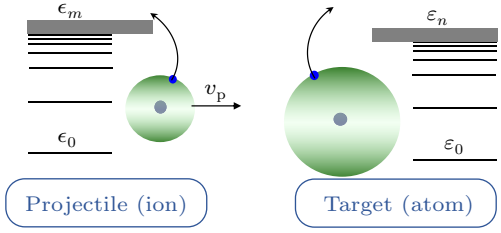


Fig. 20. Schematic illustration of the doubly inelastic transition in collision of partially striped ion with an atom.

In this section we present the theory of relativistic ion–atom collisions where the projectile-ion initially carries active electrons. We address first-order and high-order (eikonal approximation) descriptions for the projectile–electron excitation and loss in relativistic collisions with neutral atomic targets. It is shown that the influence of the higher-order effects in the projectile–target interaction on the projectile–electron excitation and loss in relativistic collisions might be considerable. We consider relativistic collisions of heavy hydrogen like ions with hydrogen and helium atoms in which the ion–atom interaction causes both colliding particles to change their internal states (see Fig. 20).

The transition amplitude, for the doubly inelastic collisions between a hydrogen like ion and an atomic target (with a single active electron model) is given by[201,202]

$$S_{fi}(Q) = -i\frac{2}{v_p}\frac{F_A^\nu(q)\gamma^{-1}\Lambda_{\mu\nu}F_I^\mu(q')}{q^2-\left[(\varepsilon_m-\varepsilon_0)^2/C^2\right]}, \tag{5}$$

where F_A^ν, F_I^μ, and $\Lambda_{\mu\nu}$ $(\mu,\nu=0,1,2,3)$ are the inelastic form factors of the target,[202] the ion and the Lorentz transformation matrix, respectively. The summation over repeated index is implied. $\boldsymbol{q}$ is the momentum transferred to the atom in the atom frame, and q' is the momentum transferred to the ion in the ion frame. They are given by $q = (Q, q^A_{min} = [(\varepsilon_n-\varepsilon_0)/v_p] + [(\varepsilon_m-\varepsilon_0)/\gamma v_p])$ and $q' = (Q, q^I_{min} = [(\varepsilon_n-\varepsilon_0)/\gamma v_p] + [(\varepsilon_m-\varepsilon_0)/v_p])$. The quantities ε_0 and ε_n are the initial and final internal energies of the atom in the frame of the atom and ε_0 and ε_m are the initial and final internal energies of the ion in the frame of the ion.

When the ion charge is much smaller than the collision velocity (atomic units are used) the doubly inelastic transition is mainly governed by the dielectronic interaction, which couples the two electrons from different centers and can be well described within the first order approaches given above. However, since $v_p < c$, the earlier condition is only fulfilled with light projectiles. As an extension to HCIs one can use a better description such as the eikonal approximation.[202] The transition amplitude for the doubly inelastic collisions between an H-like ion and a single-electron atom is given by

$$S_{fi}(\boldsymbol{Q}) = -i\frac{2}{v_p}A\int d^2\boldsymbol{p}\int d^2\boldsymbol{k}\frac{1}{p^{2-2i\eta}p^{2-2i\alpha}}\frac{F_A^\nu(\boldsymbol{q})\gamma^{-1}\Lambda_{\nu\mu}F_I^\mu(\boldsymbol{q'})}{|\boldsymbol{q}+\boldsymbol{k}-\boldsymbol{p}|^2-[(\varepsilon_m-\varepsilon_0)^2/c^2]}, \tag{6}$$

where

$$\eta = Z_pZ_t/v_p \text{ and } \alpha = Z_p/v_p,$$
$$A = \frac{\Gamma(1-i\alpha)\Gamma(0.5+i\alpha)\Gamma(1-i\eta)\Gamma(0.5+i\eta)}{4\pi^3\Gamma(2i\alpha)\Gamma(2i\eta)},$$

and $\Gamma(z)$ is the gamma function. In the expression (6) the definitions of momenta transferred either to the target $\boldsymbol{q}$ or to the projectile $\boldsymbol{q'}$ during the collision to the target, as well as definitions of the form factors are the same as given in expression (5).

Figure 21 shows the doubly differential cross section of the emitted electron from the target in a doubly inelastic collision of MeV/u $C^{5+}(1s)$ on He. As a result of the collision each of the colliding systems lose one electron. In this figure, the cross section is given for a fixed electron energy of $\varepsilon_k = 40$ eV as a function of the polar emission angle of the target electron. The result of the first-order (dashed curve), compared to the result from the eikonal approximation (solid curve) shows very substantial differences in both the magnitude and the shape of the doubly differential cross section. In particular, the eikonal approach predicts a very strong enhancement of the target emission into the backward direction and reflects the fact that the target electron does not get a large recoil in the forward direction since the momentum transfer necessary to remove the tightly bound projectile electron is provided by the target core which is a high order effect. Similar results are also obtained in longitudinal spectrum $d\sigma/dq^A_{min}$ of the doubly inelastic collisions of 100 MeV/u $Nd^{59+}(1s)$ on hydrogen shown in Fig. 22. The figure shows a significant deviation between first Born calculation (dashed curve) and the eikonal calculation (solid blue line) which includes high order effect by taking into account simultaneous both interactions: target–electron with the

projectile–nucleus and the projectile–electron with the target–nucleus which is called two-center nucleus–electron interactions. Concentrating on the study of the longitudinal momentum spectrum of the atomic recoil ions, the calculations show that the relativistic and higher order effects, can strongly influence the projectile's electron, and important information on the doubly inelastic collisions can be depicted in the recoil momentum spectrum as shown in the Fig. 22, where the peak structures depicted by the eikonal approximation correspond to the projectile electron excitation ($n = 2$ and $n = 3$) and loss to the continuum.

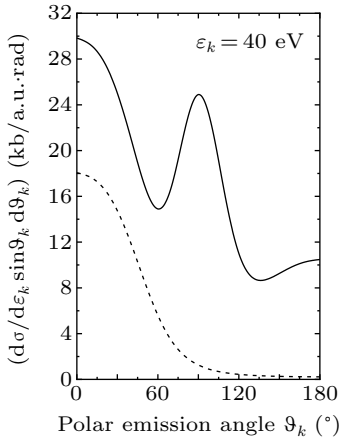


Fig. 21. $(\mathrm{d}^2\sigma/\mathrm{d}\varepsilon_k \sin\vartheta_k \mathrm{d}\vartheta_k)$ of the doubly inelastic collision of 3.6-MeV/u $C^{5+}(1s)$ on He atom. ϑ_k is the polar emission angle of the target electron with $\varepsilon_k = 40$ eV in the target frame. Dashed curve is the results of the first order calculation. Solid curve is the calculation derived from the expression (B-2) and accounts for higher order contribution.

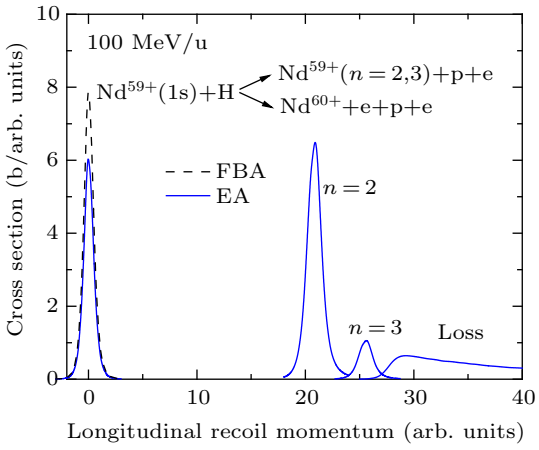


Fig. 22. The longitudinal momentum spectrum of the target recoil ions $\mathrm{d}\sigma/\mathrm{d}q_{\parallel}^{\mathrm{rec}}$ of the doubly inelastic collisions of 100-MeV/u $Nd^{59+}(1s)$ on H atom, resulting in the excitation of the projectile electron to states with $n = 2$, $n = 3$ and the projectile–electron loss. Solid (blue) and dashed curves show results of the first order and eikonal calculations, respectively.

3.4. Fragmentation dynamics in collisions of ions with molecules and small clusters

In contrast with the atomic collision processes, the molecular or cluster targets contain several nuclei bonded by strong interactions like covalent bond or weak interactions such as hydrogen bond and/or Van der Waals bond. When interacting with HCIs, multiple electrons will be removed from the target, leading to the cleavage of chemical bonds and fragmentations. Based on the coincidence detection of flight time (TOF) and position of each product, the momentum correlation among each fragment can be reconstructed. Thus, the molecular structure and its fragmentation dynamics, the focus of this section, can be investigated.

For the simple molecules consisting of three or more atoms, there are two types of fragmentation mechanisms. One is simultaneous dissociation where both bonds are disrupted concertedly, and the other mechanism is sequential dissociation, where chemical bonds break up one after the other. The Newton diagram is usually used to present the momentum correlation among each product, and to distinguish the above two mechanisms. As shown in Fig. 23, for the triple ionization of CO_2 by Ar^{8+} ion impact,[203] a circular structure is observed in the Newton diagram, which is the fingerprint of sequential dissociation, meaning that one C–O bond breaks up firstly producing an O^+ ion and a metastable ion $(CO)^{2+}$ in $^1\Pi$, $^3\Sigma$ or $2^1\Sigma$ states. Then after some rotation periods, the second fragmentation occurs, namely, the $(CO)^{2+}$ ion dissociates into C^+/O^+ ion pair. Meanwhile, a bright island is also observed in the Newton diagram, where two O^+ ions depart away back to back, and the C^+ ion locates at the low energy area. This signature agrees with the simultaneous dissociation. So far, the investigation of HCIs-induced fragmentation has been extended to other molecules like N_2O,[204] OCS,[205] and small organic molecules like C_2H_2,[206,207] C_2H_4,[208] and C_3H_4[209–211] It was found that fragmentation mechanisms and their corresponding branching ratios are dependent on the incident energy, charge state of the HCIs, and excitation state of the parent molecular ion.[203,212,213] For instance, if a molecule is triply or quadruply ionized, and the generated molecular ion lies in low excited states, the subsequent decay pathway tends to be sequential dissociation.[214]

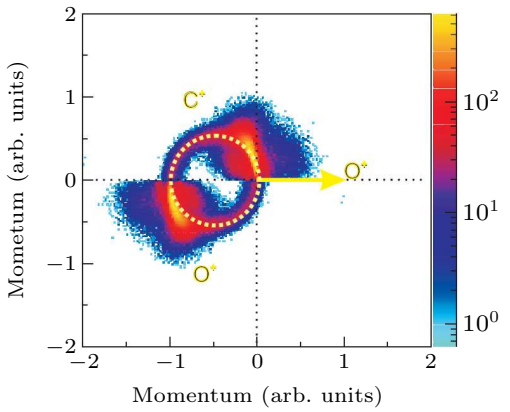


Fig. 23. Newton diagram presenting the momentum correlation among $O^+/O^+/C^+$ ions in Ar^{8+}–CO_2 collision. Reprinted figure with permission from Ref. [203].

The fragmentation dynamics of complex molecular systems, such as polycyclic aromatic hydrocarbons (PAHs), fullerenes and biological molecules,[215–221] has also received

wide attention. It is helpful to elucidate the radiation damage at the molecular level and propose new therapy scheme to reduce the side effects to healthy cells. For a complex molecule, its dissociation following ionization may involve Coulomb explosion, H migration and isomerization. Consequently, several ions and neutral fragments will be produced in each reaction and it is difficult to reconstruct all their three-dimensional momenta. Only TOF spectra are measured in most experiments, where the charge state effect is observed. Holm *et al.*,[221] investigated the fragmentation of $C_{14}H_{10}$ by 11.25-keV He^+ and 360-keV Xe^{20+} impacts, respectively. Significant difference in fragmentation has been observed for the two projectiles. The overall fragmentation probability for He^+ impact is 63%, while it decreases to 39% for Xe^{20+} impact. In addition, the Xe^{20+} collision preferentially leads to small $C_nH_x^+$ fragments with $n = 1$–5, while the H-loss and C_2H_x-loss channels are much weaker compared to He^+ impact. A similar phenomenon is observed in the fragmentation experiment of glycine NH_2CH_2COOH, the intensities of $HCNH^+$, $NH_2CH_2^+$ NH_2CH^+, $NCCO^+$, and $HNCCO^+$ ions decrease with the projectile charge increase.[216] These studies demonstrated that different mechanisms have enrolled in the HCI impact collisions. The authors attributed such difference to the multiple electron removal at large distances by Xe^{20+} due to the strong potential of highly charged projectile. The fragmentation mechanism of hydrocarbon molecules induced by charged particle collision has been widely studied by Wei's group at Fudan University, including *e.g.*, the concerted or sequential fragmentation,[208,213] lifetime of metastable dications,[222] formation mechanism of H_3^+ ions,[223] and isomerization dynamics.[224]

The investigation on cluster fragmentation provides us unique opportunities to unveil how the fragmentation dynamics are affected by the surrounding medium, an analogue to bio-environment. For the clusters consisting of small molecules, the neighboring molecule may act as a spectator, as observed in Ref. [225] for $(N_2)_2$. Nevertheless, it can also induce a fast dissociation pathway which enhances the fragmentation of its neighbor, as observed in Ref. [226]. For the clusters containing complex molecules, because of the large number of internal degrees of freedom, it is expected that, the excess energy and charge transferred from the projectile to the cluster can be dissipated through intermolecular-bond cleavage within the cluster, thus, protecting the molecule against breaking into small fragments, which may be an example for protection of the biological molecule against serious fragmentations in irradiation. This expectation is identified in some gas-target experiments induced by ion impact, and further confirmed by the aqueous system.[19,227,228] However, only one exception was observed, as shown in Fig. 24, the overall TOF spectrum of $C_{14}H_{10}$ cluster after Xe^{20+} ion impact is similar to that of the isolated molecule by He^+ ion impact, which means the protective effect is not obvious and significant excess energy is fed into the $C_{14}H_{10}^+$ ion favoring its further fragmentation.

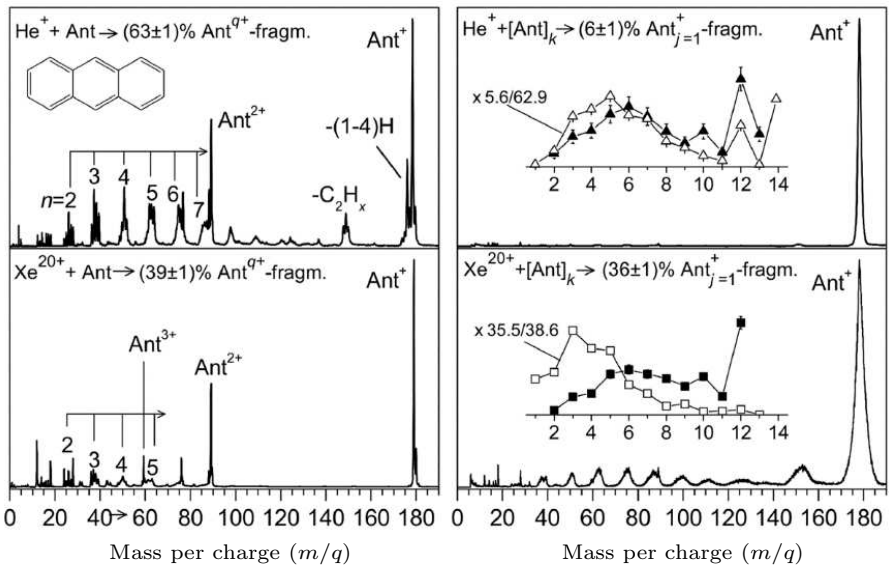


Fig. 24. TOF spectra after collision between ion and anthracene $C_{14}H_{10}$ molecule (Ant) or its cluster: right: collision between He^+/Xe^{20+} ion with Ant molecule, left: collision between He^+/Xe^{20+} ion with Ant cluster. Reprinted figure with permission from Ref. [221].

A more interesting scenario is that the impact of HCIs can initiate not only fragmentation with bond cleavage but may also lead to the formation of new chemical bonds. Figure 25 shows the intermolecular relaxation processes of acetylene dimer (C_2H_2–C_2H_2), a biologically relevant system possessing an intermolecular hydrogen bond, investigated by 200 keV/u He^{2+} impact.[19] Two fragmentation channels of the charged dimer are identified. The first one is the already well-established interatomic Coulomb decay (ICD) of inner-valence-ionized states. Its occurrence after ionization of the

shallow carbon 2s levels has been identified, highlighting the importance of ICD in organic systems. The other is a novel relaxation mechanism of dicationic states, which involves intermolecular proton transfer and formation of new CH bond, namely, the final channel appears as $C_2H^+ + C_2H_3^+$. Both processes are very fast and trigger Coulomb explosion of the dimer due to creation of charge-separated states. The important and new finding is that the addressed proton transfer process constitutes a general phenomenon in hydrogen-bonded systems like ICD. They are expected to take place in alpha-particle-irradiated DNA and thus cause damage to this biomolecule, as shown in the lower panel of Fig. 25.

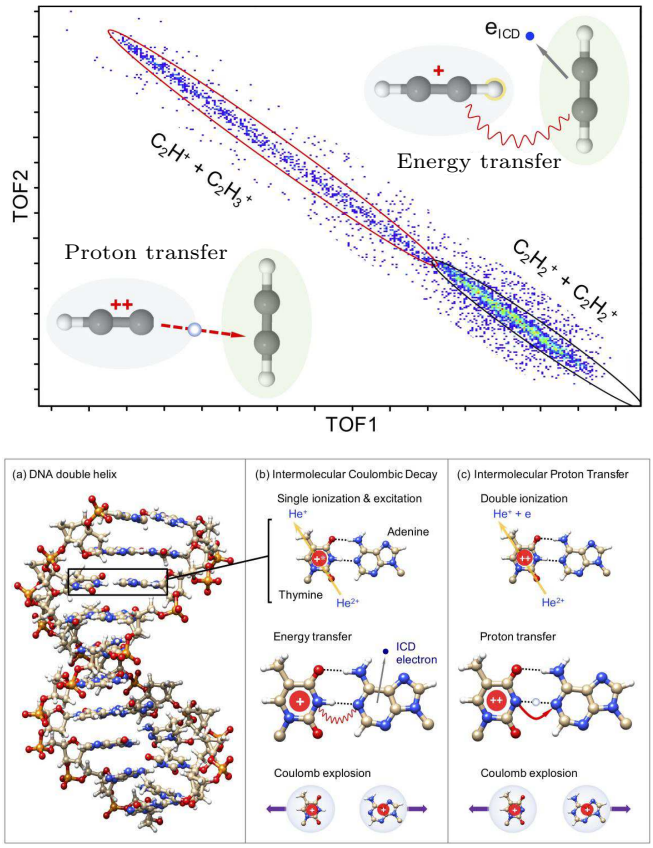


Fig. 25. Upper panel: Time-of-flight coincidence map corresponding to the two-body breakups of acetylene dimers. The contribution of the $C_2H^+ + C_2H_3^+$ channel with intermolecular proton transfer is indicated by the red oval. The black oval contains the contribution of the $C_2H_2^+ + C_2H_2^+$ channel mainly arising from ICD. Upper panel: Similar decay mechanisms may also occur in bio-systems like DNA base pair. Reproduced with permission from Ref. [19].

In a consequent study, the neutral vdW cluster N_2Ar was used as a target in collisions with 1-MeV Ne^{8+} ions to produce the doubly charged cluster $(N_2Ar)^{2+}$. Surprisingly, an exotic heavy N^+ ion transfer channel $(N_2Ar)^{2+} \rightarrow N^+ + NAr^+$ was observed.[20] It is the first time that such a heavy-ion transfer process in a vdW cluster has ever been reported and the consequent formation of NAr^+ is a novel scenario. According to the study, this channel originates from the dissociation of the parent doubly charged cluster $N_2^{2+}Ar$ generated by the two-electron loss process at "N_2-site". Theoretical calculations show that the polarization interactions between Ar and N_2^{2+} lead first to an isomerization process of $N_2^{2+}Ar$ from its initial T-shape to a linear shape (N–N–Ar). In addition, the neighboring neutral Ar atom decreases the N_2^{2+} barrier height and width, resulting in significantly shorter lifetimes for the metastable electronic state. Consequently, the breakup of the covalent N^+–N^+ bond, the tunneling out of the N^+ ion from the N_2^{2+} potential well, as well as the formation of the N–Ar^+ bound system take place almost simultaneously. Then the Coulomb explosion starts between N^+ and NAr^+ ion pairs. The detailed information of the process could be seen in Fig. 26. This new mechanism might be general for molecular dimer ions in the presence of a neighboring atom, and be of potential importance in understanding the microdynamics of biological systems. For example, it may be helpful to understand the micromechanism of cancer therapy by heavy ion irradiation.

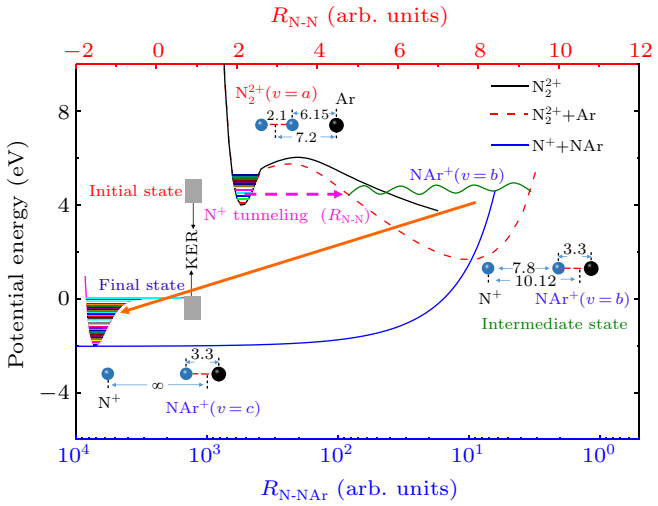


Fig. 26. Schematic diagram of heavy ion transfer process through tunneling.[20] Reproduced with permission from Ref. [20].

Compared with the sequential dissociation, protective effect, intermolecular proton migration, and bond formation discussed above, a more remarkable feature of HCI is its strong Coulomb potential and its strong capability to remove multiple electrons from atoms or molecules. Indeed, HCIs may remove five-, ten-, or even more electrons from a target, leading to the instant Coulomb explosion of multiply charged parent molecules. Since the swift and large distance collision is a soft process and will leave the parent molecular ion to ground or low excited state, avoiding the change of its initial geometry. The fast fragmentation is purely driven by Coulomb repulsion.[229] Therefore, by measuring the final momentum of each fragments, it is possible reconstruct the initial geometry of the neutral molecule and cluster. This type of Coulomb explosion imaging technique is more accurate and reliable than the fragmentation method using strong laser field.[214]

Theoretical treatments of molecular fragmentation induced by charged particles or lasers are a challenging task. The group in the Institute of Applied Physics and Computational Mathematics (IAPCM) has developed systematic theoretical methods to treat the highly charged ion structures and related collisions dynamics processes, in which one main challenge is to construct the high-dimensional potential energy surface (PES) of the involved highly excited electronic states. Recently, in combination with the multi-reference double-excitation configuration interaction method[230] and multi-configurational self-consistent-field approach, IAPCM group developed an *ab initio* method[231] and the PESs can be computed with a relatively high precision. Furthermore, they developed a semi-classical Landau–Zener surface hopping method (LZSH)[229] and a full quantum time-dependent wave-packet evolution method (TDWP)[232] to treat the multi-body breakups of highly charged polyatomic molecules. In the LZSH method, the simulations are performed based on the high-accuracy 3D PESs calculations and the transition between different electronic states can be considered reasonably with the Landau–Zener transition probabilities[229] in the fragmentation process and the correlation among charged fragments. In the TDWP method, the interaction picture theory was used to propagate the wave packet, and the effects of strong and long-range interactions can be considered by basis functions and the weak and short-range interactions are included in the perturbation term, in which the Coulomb interactions, polycentric interactions, vibration-rotation coupling of molecular fragments, and the rotation-rotation coupling between molecular fragment and parent molecule can be considered accurately.[232] With the LZSH and TDWP methods, extensive studies have been performed and some interesting phenomena have been found in the ion induced fragmentation processes of polyatomic molecules. For example, in the two-body breakups of molecular dimers, it is found that the molecular fragments can rotate rapidly under the influence of neighbor ion[229,232] and such an ultrafast rotation mechanism is revealed to be a general phenomenon in the breakups of polyatomic molecule, which are dominated by the polycentric interaction between fragments and impacted by the vibration-rotation and rotation–rotation couplings. These methods were also extended to study the pump-probe experiments, for examples, the real-time bond-breaking dynamics of OCS^+ caused by radial coupling interaction[233] and the photon-induced ultrafast processes of the SO_2.[234]

3.5. Phase information in collision processes

Young's double-slit interference is a clear manifestation of the wave character of light and is easily demonstrated experimentally. An analogous double slit experiment to prove the wave nature of a massive particle as postulated by DeBroglie in 1925 is not straight forward because its DeBroglie wavelength is tiny, and no mechanical double slit can match the wavelength. Indeed, the first evidence for this hypothesis did not come from such a double slit experiment, but rather from the interference effects in electron scattering from metal surfaces.[235] It took another three decades before the realization of an atomic version of Young's double slit experiment in ion–atom collisions, which was first discussed theoretically by Tuan and Gerjuoy in 1960.[236] They suggested that diffraction of a proton from the two atomic centers of the molecule H_2 could lead to observable interference effects. Only recently the predictions of Tuan and Gerjuoy were confirmed by several experiments where variations of the capture cross sections as a function of the molecular orientation could be attributed to the interference effects.[237–239]

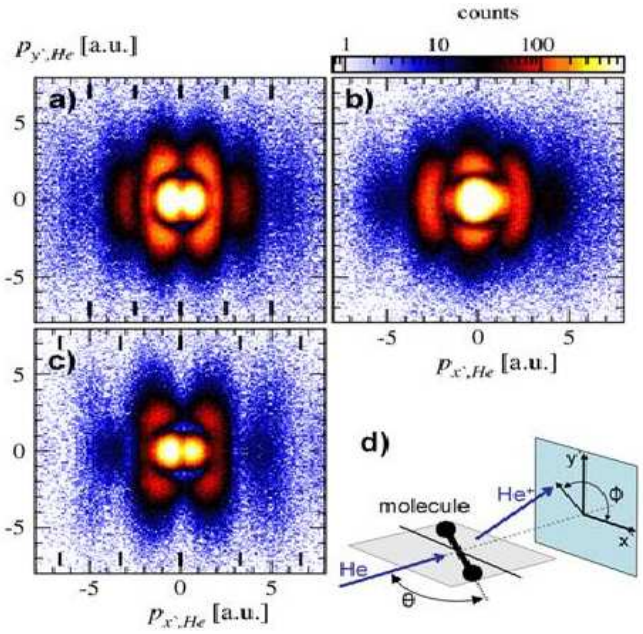


Fig. 27. Interference patterns observed in capture collisions between H_2^+ and He.[240] The spectra are token in the molecular rest frame where the molecular axis is along the X axis. (a) and (c) The molecular axis is perpendicular to the projectile direction and the internuclear distances are 2.6 a.u. and 1.85 a.u. respectively; (b) the polar angle $\theta = 55^\circ$ and the internuclear distance is the same as in panel (a). Reproduced with permission from Ref. [240].

Pronounced interference fringes similar to those in the optical double-slit experiments were reported by Schmidt *et al.* in 2008.[240] In their work the hydrogen molecular ion H_2^+ was used as the 'double-slit' and the recoil ion momentum spectra are studied in the rest frame of the molecular ion after the electron capture induced dissociation. It is found that in the molecular frame the recoil ion momentum spectra present clear alternating structures along the molecular axis as shown in Fig. 27 and the period of oscillation agrees well with the predictions, in which the DeBroglie wave of helium atom scattered on the double slit of a width the same as the internuclear distance along the molecular axis. In their studies an additional phase shift of π, resulting from the parity changes

of molecular states, is found entering in the phase angle of the interference term and thus, the extrema of the interference fringes are flipped.

Interference effects in projectile diffraction are more challenging to be observed in ionization processes.[241] Since the final state of the collision involves at least three unbound particles, the experimental determination of the momentum-balance in the collision, which enters in the phase angle of the interference term, is more demanding compared to that of the capture processes. Data for ionization in which the phase angle was completely determined was firstly reported for electron impact, however, interference effects can hardly be extracted from the spectra.[242] For ion impact, interference in projectile diffraction was observed for fixed projectile energy losses in the scattering angle spectra.[243,244] There, the recoil-ion momentum was not analyzed resulting in an averaging over the phase angle. This averaging led to a damping of the interference pattern but did not eliminate it.

The first experiment in which all phase angle information is completely determined was reported in 2014.[245] In the work the same colliding system as in Ref. [239] was employed, however, target atom ionization was studied, and the momentum of the ejected electron as well as that of the recoil were measured with high precision. Interference patterns analogous to the optical experiment are unambiguously identified from cross sections differential in the transverse momentum transfer except for the flipped extrema due to a similar reason in Ref. [239] (see Fig. 28).

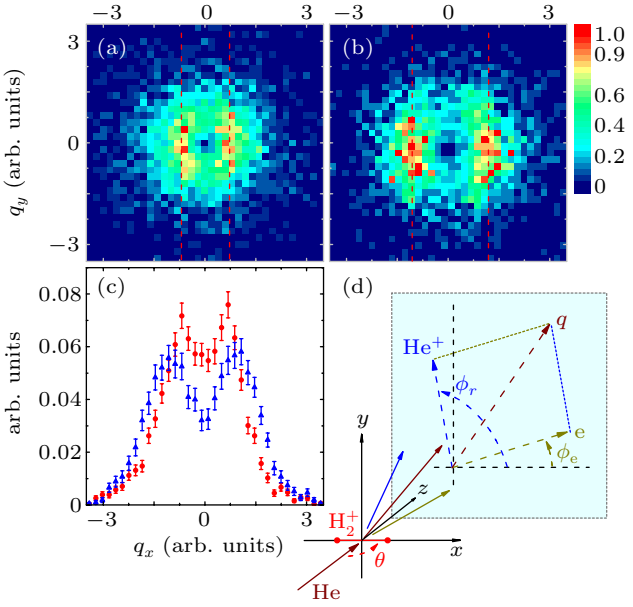


Fig. 28. Interference patterns observed in ionization processes in collisions between H_2^+ and He.[245] Panels (a) and (b) represent the case when the molecular axis is perpendicular to the projectile direction meanwhile the internuclear distances are 3.6 a.u. and 1.7 a.u., respectively; panel (c) shows the X-axis projection of panels (a) and (b). Reproduced with permission from Ref. [245].

Although the interference fringes in both Ref. [239] and Ref. [245] display similar minima structure at zero angle along the X axis, their mechanisms are different. In the case of Ref. [239] the electron is captured from the one-center $1s^2$ state of the helium atom to the two-center asymmetric $2p\sigma_u$ state of the hydrogen molecule. The interference phenomena can thus be understood as the active electron jumps from a one-center state to a superposition state where two undistinguished paths exist. While in the case of Ref. [245], there is no charge exchange between the colliding partners, but the interactions between the ionized electron from the helium atom and the only electron in the hydrogen molecular ion establish two paths which cannot be distinguished since we do not know to which center of the hydrogen molecular ion the molecular electron belongs. In both cases, the symmetry of the electronic wavefunctions alters from the 'gerade' to 'ungerade' which leads to the shift of π in the interference phase angle of scattered matter wave which causes the flips of the extrema accordingly.

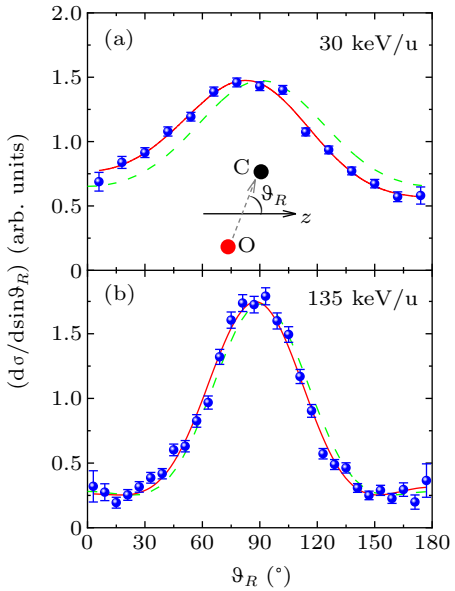


Fig. 29. Molecular orientation dependent cross sections in collisions of He^{2+} and Co.[21] The polar angle ϑ_R is defined by the angle between the projectile direction and the molecular axis vector pointing from the oxygen center to the carbon center. $\vartheta_R = 90°$ represents the case that the molecular axis is perpendicular to the projectile direction. Panel (a) for collision energy of 30 keV/u and panel (b) for 135 keV/u. The red solid line is the fitting to the experimental data with $\sigma[1+\cos(\phi\cos\vartheta_R+\Delta')]$ where σ, ϕ, and Δ' are free parameters, meanwhile the corresponding green dashed line is the simulation with the same σ and ϕ, but keep $\Delta' = 0$ (the non phase shift case). Reproduced with permission from Ref. [21].

In the studies mentioned above, the symmetric diatomic molecule of H_2 is employed as the double-slit. It is thus nature to ask the question 'what will the interference fringes look like if the asymmetric molecules are used instead?'. Recently, Gao *et al.*,[21] performed an experiment utilizing the asymmetric molecule CO as the double-slit and scrutinized the interference effects in the capture collisions with He^{2+} impact. It is found that the interference feature is surprisingly different from those with symmetric molecules. As shown in Fig. 29, they observed the asymmetric angular distribution about 90 degrees

in the polar angle spectra defined by the molecular axis and the projectile incident direction. This asymmetry is ascribed to different phases of He^{2+} ion scattering on the carbon and oxygen atomic centers and, for the first time, the phase information in ion–atom collision processes was extracted. Phase information in collision processes not only provides the most stringent test of theory but also opens the prelude to new areas of atomic collision studies.

In brief, based on the reaction microscope double-slit experiments in ion–molecule collisions have exhibited great potentials to advance our knowledge in the field. On one hand, it inaugurates a new direction of ion–atom collisions. For instance, the scattering phase of ion–atom collision processes can be extracted out from the shifts in the interference fringes which cannot be accessed before. On the other hand, the kinematically complete experiments on the simplest interference processes with massive particles also extend our ability to explore the deeper principles underlying the uncertainty and nonlocal realism in the near future (see Section 4).

4. Conclusions and prospects

In this review, we have reported on the progresses on the studies of structure of highly charged ions and the collision dynamics of HCIs with atoms, molecules and clusters, based on accelerator storage rings and the electron beam ion traps mainly in recent twenty years. Further, there is even more to be excited about, new generation accelerator facilities are being under construction around the world to make full use of highly charged ions in atomic physics research, such as the facility for antiproton and ions research (FAIR)[246] in Darmstadt Germany, the high intensity heavy ion accelerator facility (HIAF)[52] in Huizhou city China, and the nuclotron-based heavy-ion collider facility (NICA)[247] in Dubna Russia. All these facilities will exclusively provide high quality beams of highly charged ions and unprecedented experimental conditions for structure and collision dynamics studies in strong electromagnetic fields, at higher impact velocities and with more intense HCI beams. In the following we try to give some possible proposals for future investigations employing HCIs at the current and future facilities.

With the improvements of momentum resolution, reaction microscope may also be used as a tool for spectroscopy, thus, there is no distinct border for the structure and dynamics studies using experimental methods discussed in the present cases. Therefore, the future prospects related to structure and collision dynamics will be discussed together. From the aspects of collision dynamics, in the review paper of Döner[6] and Ullrich,[7] many good ideas have been proposed concerning the research using reaction microscopes, some of which are still in preparations. Here, we will present some new proposals rather than simply repeating their points.

(i) Nonlocal realism studies with quantum gratings in relativistic collisions

One of the attractive aspects in studies of ion–atom/molecule collision dynamics is definitely belonging to new opportunities that the massive relativistic ion can bring to us. For instance, in 1935, Einstein, Podolsky, and Rosen argued that the quantum theory violates the local realism and thus cannot be complete.[248] By 'local realism', they claimed that the physical properties of an object are independent of the measurement applied on it (realism) and the physical influence cannot propagate faster than the speed of light (locality). Later in 1964, Bell proved that no theory based on Local Realism can give the same predictions as those from the quantum theory.[249] So far, the 'loophole'-free experiment has confirmed the nature property of the non-local reality.[250] However, the origin of such property still remains as one of the most fundamental problems in quantum physics. According to the relativistic theory, the ion of relativistic velocities will see a much slower time flow in the rest frame which is known as the time dilation. With the quantum grating consisting of a single atom proposed in Ref. [22] as shown in Fig. 30, the kinematically complete studies of relativistic collisions might be able to spell out more information on the nonlocalities of the quantum objects.

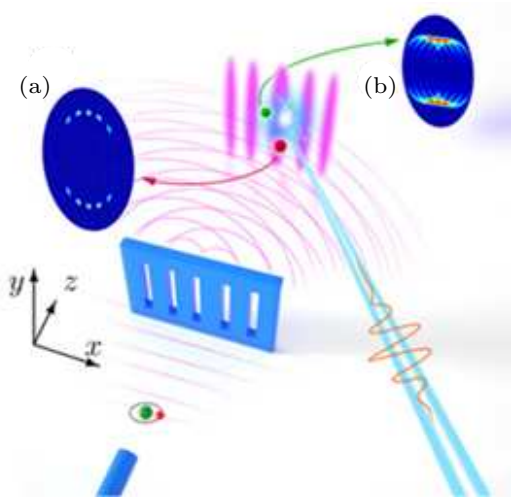


Fig. 30. Schematic diagram of a 'quantum grating' prepared by a single atom.[22] Reproduced with permission from Ref. [22].

(ii) Population of spin states in charge exchange processes

The high resolution of the reaction microscope already enables one to access the spin states in single electron capture process at not very high collision velocities. Traditionally, the population of spin states are studied by photon spectroscopy, where one has to measure the photon emission angular distribution and deduce the information of spin state population. One of the difficulties is the low detection efficiency in this kind of measurements and thus, available experimental data are rare. However, with high-resolution reaction microscope/COLTRIMS, it is possible to measure SEC into differ-

ent spin states and to obtain directly information on spin state populations.

(iii) Determination of the energy of doubly excited states

A further advantage of the high-resolution reaction microscope is the access to the multiply excited states in electron capture processes. For example, the doubly excited states formed in DEC, which could be embedded in the continuum or in bound states. The energy of the doubly excited states can be investigated via Auger decay by detecting autoionized electron in the first case. However, it is extremely difficult to determine its energy in the second case because it needs to detect all the emitted photons in cascades. The reaction microscope/COLTRIMS can, on the contrast, extract the level energy directly from recoil ion momentum, no matter what a doubly excited state decays via Auger or radiation.

(iv) Direct measurements of Lamb shift of 1s ground state for hydrogen-like ions

Test of bound state QED using HCIs in strong EM field is mainly conducted via photon detection technique, in most cases the transition energy of Lyman transitions are detected using solid state Ge(i) detector.[112] At the electron cooler of storage ring, the transition energy of radiative recombination of a free electron with bare heavy ions was also measured at near zero observation angles, and the 1s binding energy is directly deduced. However, one of the main uncertainties is from Doppler effect, which exists in photon detection for all accelerator-based experiments. Using high resolution reaction microscope, the 1s binding energy of hydrogen like ions can be extracted from recoil ion momentum in single electron capture in, *e.g.* bare heavy ion–helium atom collisions, where the binding energy of helium atom is known with high accuracy. The most remarkable point in the methods is that the Doppler effect does not appear and the absolute value of the 1s energy level could be determined, and the accuracy will be comparable or better than x-ray spectroscopy. This method will be an independent check to the method of photon detection.

(v) Spontaneous e^+e^- pair creation in super critical EM fields

Quantum electrodynamics (QED) is the basis of modern field theory and standard model. Bound state QED has been tested by the most rigorous experiments in weak electromagnetic fields, *e.g.* the 1s Lamb shift in hydrogen atom. However, its applicability in strong field is facing challenge and is tested only at the level of about 1% up to date, due to the restrictions of experimental conditions. On the other hand, quantum field theory predicts that when the field strength reaches or exceeds the critical value of about 1.3×10^{16} V/cm, the neutral vacuum will decay through the spontaneous electron–positron pair creation, but it has not been verified by experiments to date. One of the scientific goals of China's new large scale facility HIAF is to build a merging beam collision storage ring MRING,[52] which will create an ideal platform for two bare heavy ion beams colliding with low energy at the central of mass (CM) system under low background for the first time in the world. The experiment will identify the spontaneous positron-electrons pairs created in vacuum decay beyond Schwinger's critical field and will confirm the vacuum decay in supercritical Coulomb field, or find new physics beyond the current QED theory. In the same period, GSI/FAIR in Germany[246] and NICA in Dubna Russia[247] also plan to carry out relevant research. Furthermore, with bare and H-like ion collisions, the quasi-molecular processes could be investigated in extremely strong EM fields.

(vi) Collisions between two extreme systems: giant dimers versus ultrafast HCIs

Collisions of ultrafast HCIs with atomic/molecular targets not only enable one to get a better insight into the relativistic collision physics, but also, it may provide a valuable information on the structure of the extended target, such as He_2 dimer, and thus, probe its binding energy. Recently, it was shown[227] that, due to their extreme long interaction-range, relativistic HCIs, in collisions with He_2 dimer, can be used to probe the structure of the dimer ground state, particularly in the quantum halo region ($\sim$ 14 Å–280 Å, classically forbidden region) where the dimer spends more than 80% of the time and its radial wave function is directly related to its binding energy. Hence, ultrafast HCIs can be used as a tool to determine the binding energy of the dimer as well as weakly bound systems.

(vii) Ion induced chemistry in the universe

Heavy ion atomic collisions have potential advantages of populating and depleting new quantum states and easily transferring a large amount of energy at very short interaction time. The ion-neutral chemistry induced by these collisions can facilitate the gas-phased chemical reactions that are mostly hindered by the potential barrier between neutrals.[251,252] Therefore, heavy ion atomic collisions may open up new cutting-edge chemistry studies, which are, in particularly, associated with the complicated and exotic molecule formation in interstellar space.

(viii) Decay mechanisms of bio-systems induced by HCIs

Heavy ion beam cancer therapy has been applied to clinical treatments. However, the interaction mechanisms at molecular level are still unclear, although several possible processes like ICD, inter-molecule proton or heavy ion transfer[19,20] have been identified. Therefore, the studies of fragmentation mechanism of bio-targets like DNA base pairs and bio-water clusters induced by HCIs will shed more light for our understanding of the micro-mechanisms of radiation damage and cancer therapy.

(ix) Nuclear excitation via electron capture

A nuclear state could be excited when an electron is captured into the ion bound state, analogous to DR process, this is

the so-called nuclear excitation via electron capture (NEEC). One of the hot topics related to nuclear clock is to measure the low nuclear excitation energy in Thorium-229, whose first excited level is around 8.28 ± 0.17 eV.[253] NEEC may be employed to measure this small transition energy with high accuracy at the electron cooler of storage rings.[254] Furthermore, at the future facility HIAF, an independent electron target will be installed and the collision energy at CM frame up to hundred keV will be accessible, thus, the NEEC method can be used to determine nuclear transition energies at the accuracy of atomic spectroscopic levels.

(x) DR spectroscopy with radioactive nuclei

With the upgrade of the capability of radioactive ion production, intense unstable nuclear beams can be injected into the storage rings for experiments in near future. It has already been demonstrated that DR technique could be used to obtain nuclear properties,[26] such as isotope shift, nuclear charge radii, isomeric state, *etc*. These measurements will be realized in the next ten years at the future accelerator facilities like FAIR and HIAF.

(xi) DR spectroscopy with ions in metastable states

There are metastable ions in various plasmas and they may contribute to the charge balance, plasma evolution, *etc*. However, it is difficult to measure the corresponding atomic parameters, such as DR rates, due to the lack of enough amount of metastable ions prepared for experiments. New hopes appear as the storage ring in operation. The metastable ions produced in ion source could be delivered and stored in the storage ring for DR studies, a test experiment at the CSRm has been demonstrated and can be found in Ref. [39].

(xii) Strong electron correlation and two-electron one photon decay

One of exotic atomic processes is two-electron one photon (TEOP) decay, here focused is the decay with two K-shell core holes filled simultaneously via a correlated two-electron jump and one photon emission, which attracts interest in past decades.[255] Unlike direct x-ray photon detection,[256] where detection efficiency and statistics are poor, the interference between DR and RR processes could be employed as a signature to detect the TEOP decay. At storage rings, this method has advantages to prepare two electrons in L-shell with two K-shell vacancies using hydrogen-like ions through DR excitation and to study the $2l2l'$-$1s^2$ TEOP decay. A recent theoretical paper points out that DR–RR interference occurs with high probability in light ion systems.[257]

(xiii) Laser-assisted relativistic ion–atom collisions

It is expected that, in the presence of an external electromagnetic field, atomic scattering processes involving incident photons and electrons can be modified substantially.[258] A new theoretical study shows that a circularly polarized low-frequency electromagnetic field can qualitatively change the shape of the spectra of the emitted high-energy electrons due to a very large energy exchange between the electron and the field in relativistic ion–atom collision.[258] The experimental studies of laser-assisted binary-encounter emission in relativistic ion–atom collisions could be expected at storage rings.[175]

(xiv) Stereo Coulomb explosion imaging of complicated molecules and weakly bound clusters

The interaction time between a high energy HCI and molecules could be as short as 10^{-18} s–10^{-21} s, and in the meantime, the HCI can easily remove multiple electrons from target species, leading to highly charged molecules or clusters populated to low lying states or ground states. The highly charged molecule/cluster will explode instantly due to Coulomb repulsion. With the ability of multi-detection of charged fragments of reaction microscope, three-dimensional imaging of the molecule/cluster would be realized through the reconstruction of the momentum of each fragment. One advantage in HCI-molecule collision is direct formation of multiply charged parent molecules and consequent fast breakup, compared to synchrotron and strong laser experiments.

Acknowledgments

Project supported by the National Key Research and Development Program of China (Grant No. 2017YFA0402300), the Strategic Priority Research Program of the Chinese Academy of Sciences (Grant No. XDB34020000), and the Heavy Ion Research Facility in Lanzhou (HIRFL).

References

[1] Karshenboim S G, Pavone F S, Bassani G F, Inguscio M and Hänsch T W 2001 *The Hydrogen Atom, Precision Physics of Simple Atomic System* (Springer)
[2] Steck M and Litvinov Y A 2020 *Prog. Part. Nucl. Phys.* **115** 103811
[3] Marrs R E, Elliott S R and Knapp D A 1994 *Phys. Rev. Lett.* **72** 4082
[4] Mokler P H 1998 *Hyperfine Interact.* **114** 21
[5] Schulz M, Moshammer R, Fischer D, Kollmus H, Madison D H, Jones S and Ullrich J 2003 *Nature* **422** 48
[6] Dörner R, Mergel V, Jagutzki O, Spielberger L, Ullrich J, Moshammer R, and Schmidt-Böcking H 2000 *Phys. Rep.* **330** 95
[7] Ullrich J, Moshammer R, Dorn A, Dörner R, Schmidt L P H and Schmidt-Böcking H 2003 *Rep. Prog. Phys.* **66** 1463
[8] Mergel V, Dörner R, Achler M, Khayyat K, Lencinas S, Euler J, Jagutzki O, Nüttgens S, Unverzagt M, Spielberger L, Wu W, Ali R, Ullrich J, Cederquist H, Salin A, Wood C J, Olson R E, Belkić D, Cocke C L and Schmidt-Böcking H 1997 *Phys. Rev. Lett.* **79** 387
[9] Dörner R, Khemliche H, Prior M H, Cocke C L, Gary J A, Olson R E, Mergel V, Ullrich J and Schmidt-Böcking H 1996 *Phys. Rev. Lett.* **77** 4520
[10] Schmidt L P H, Goihl C, Metz D, Schmidt-Böcking H, Dörner R, Ovchinnikov S Y, Macek J H and Schultz D R 2014 *Phys. Rev. Lett.* **112** 083201
[11] Stolterfoht N, Havener C C, Phaneuf R A, Swenson J K, Shafroth S M and Meyer F W 1986 *Phys. Rev. Lett.* **57** 74
[12] Zhang R T, Feng W T, Zhu X L, Zhang S F, Guo D L, Gao Y, Qian D B, Xu S, Yan S C, Zhang P, Huang Z K, Wang H B, Hai B, Zhao D M and Ma X 2016 *Phys. Rev. A* **93** 032709
[13] Moshammer R, Schmitt W, Ullrich J, Kollmus H, Cassimi A, Dörner R, Jagutzki O, Mann R, Olson R E, Prinz H T, Schmidt-Böcking H and Spielberger L 1997 *Phys. Rev. Lett.* **79** 3621

[14] Weber T, Weckenbrock M, Staudte A, Spielberger L, Jagutzki O, Mergel V, Afaneh F, Urbasch G, Vollmer M, Giessen H and Dörner R 2000 *Phys. Rev. Lett.* **84** 443

[15] Bergues B, Kübel M, Johnson N G, Fischer B, Camus N, Betsch K J, Herrwerth O, Senftleben A, Sayler A M, Rathje T, Pfeifer T, Ben-Itzhak I, Jones R R, Paulus G G, Krausz F, Moshammer R, Ullrich J and Kling M F 2012 *Nat. Commun.* **3** 813

[16] Schöffler M S, Stuck C, Waitz M, Trinter F, Jahnke T, Lenz U, Jones M, Belkacem A, Landers A L, Pindzola M S, Cocke C L, Colgan J, Kheifets A, Bray I, Schmidt-Böcking H, Dörner R and Weber T 2013 *Phys. Rev. Lett.* **111** 013003

[17] Kircher M, Trinter F, Grundmann S, Vela-Perez I, Brennecke S, Eicke N, Rist J, Eckart S, Houamer S, Chuluunbaatar O, Popov Y V, Volobuev I P, Bagschik K, Piancastelli M N, Lein M, Jahnke T, Schöffler M S and Dörner R 2020 *Nat. Phys.* **16** 756

[18] Gao J W, Wu Y, Sisourat N, Wang J G and Dubois A 2017 *Phys. Rev. A* **96** 052703

[19] Xu S, Guo D, Ma X, Zhu X, Feng W, Yan S, Zhao D, Gao Y, Zhang S, Ren X, Zhao Y, Xu Z, Dorn A, Cederbaum L S and Kryzhevoi N V 2018 *Angew. Chem. Int. Ed.* **57** 17023

[20] Zhu X, Hu X, Yan S, Peng Y, Feng W, Guo D, Gao Y, Zhang S, Cassimi A, Xu J, Zhao D, Dong D, Hai B, Wu Y, Wang J and Ma X 2020 *Nat. Commun.* **11** 2987

[21] Gao Y, Zhang S, Zhu X, Guo D, Schulz M, Voitkiv A, Zhao D, Hai B, Zhang M and Zhang R 2018 *Phys. Rev. A* **97** 020701

[22] Zhang S F, Najjari B and Ma X 2021 *J. Phys. B: At., Mol. Opt. Phys.* **54** 15

[23] Beiersdorfer P, Hell N and Lepson J K 2018 *Astrophys. J.* **864** 24

[24] Preval S P, Badnell N R and O'Mullane M G 2016 *Phys. Rev. A* **93** 042703

[25] Brandau C, Kozhuharov C, Müller A, Shi W, Schippers S, Bartsch T, Böhm S, Böhme C, Hoffknecht A and Knopp H 2003 *Phys. Rev. Lett.* **91** 073202

[26] Brandau C, Kozhuharov C, Harman Z, Müller A, Schippers S, Kozhedub Y S, Bernhardt D, Böhm S, Jacobi J, Schmidt E W, Mokler P H, Bosch F, Kluge H J, Stöhlker T, Beckert K, Beller P, Nolden F, Steck M, Gumberidze A, Reuschl R, Spillmann U, Currell F J, Tupitsyn I I, Shabaev V M, Jentschura U D, Keitel C H, Wolf A and Stachura Z 2008 *Phys. Rev. Lett.* **100** 073201

[27] Schippers S, Schmidt E W, Bernhardt D, Yu D, Muller A, Lestinsky M, Orlov D A, Grieser M, Repnow R and Wolf A 2007 *Hci* 2006*:* 13*th International Conference on the Physics of Highly Charged Ions* **58** 137

[28] Lestinsky M, Lindroth E, Orlov D, Schmidt E, Schippers S, Böhm S, Brandau C, Sprenger F, Terekhov A and Müller A 2008 *Phys. Rev. Lett.* **100** 033001

[29] Müller A 2008 *Adv. At. Mol. Opt. Phys.* **55** 293

[30] Schippers S 2015 *Nucl. Instrum. Method B* **350** 61

[31] Brandau C, Kozhuharov C, Lestinsky M, Müller A, Schippers S and Stöhlker T 2015 *Phys. Scr.* **T166** 014022

[32] Schuch R and Böhm S 2007 *J. Phys. Conf. Ser.* **88** 012002

[33] Lestinsky M, Andrianov V, Aurand B, Bagnoud V, Bernhardt D, Beyer H, Bishop S, Blaum K, Bleile A and Borovik A 2016 *Eur. Phys. J. Spec. Top.* **225** 797

[34] Grieser M, Litvinov Y A, Raabe R, Blaum K, Blumenfeld Y, Butler P A, Wenander F, Woods P, Aliotta M and Andreyev A 2012 *Eur. Phys. J. Spec. Top.* **207** 1

[35] Bernhardt D, Brandau C, Harman Z, Kozhuharov C, Böhm S, Bosch F, Fritzsche S, Jacobi J, Kieslich S and Knopp H 2015 *Phys. Rev. A* **91** 012710

[36] Brandau C, Kozhuharov C, Müller A, Bernhardt D, Banas D, Bosch F, Currell F, Dimopoulou C, Gumberidze A and Hagmann S 2013 *Phys. Scr.* **T156** 014050

[37] Shevelko V and Tawara H 2012 *Atomic Processes in Basic and Applied Physics* (Heidelberg, Springer-Verlag) p. 283

[38] Huang Z K, Wen W Q, Wang H B, Xu X, Zhu L F, Chuai X Y, Yuan Y J, Zhu X L, Han X Y, Mao L J, Li J, Ma X M, Yan T L, Yang J C, Xiao G Q, Xia J W and Ma X 2015 *Phys. Scr.* **T166** 014023

[39] Wang S X, Xu X, Huang Z K, Wen W Q, Wang H B, Khan N, Preval S P, Badnell N R, Schippers S, Mahmood S, Dou L J, Chuai X Y, Zhao D M, Zhu X L, Mao L J, Ma X M, Li J, Mao R S, Yuan Y J, Tang M T, Yin D Y, Yang J C, Ma X and Zhu L F 2018 *The Astrophys. J.* **862** 134

[40] Khan N, Huang Z K, Wen W Q, Mahmood S, Dou L J, Wang S X, Xu X, Wang H B, Chen C Y and Chuai X Y 2018 *Chin. Phys. C* **42** 064001

[41] Huang Z K, Wen W Q, Wang S X, Khan N, Wang H B, Chen C Y, Zhang C Y, Preval S P, Badnell N R, Ma W L, Liu X, Chen D Y, Zhu X L, Zhao D M, Mao L J, Ma X M, Li J, Tang M T, Mao R S, Yin D Y, Yang W Q, Yang J C, Yuan Y J, Zhu L F and Ma X 2020 *Phys. Rev. A* **102** 062823

[42] Huang Z K, Wen W Q, Xu X, Mahmood S, Wang S X, Wang H B, Dou L J, Khan N, Badnell N R, Preval S P, Schippers S, Xu T H, Yang Y, Yao K, Xu W Q, Chuai X Y, Zhu X L, Zhao D M, Mao L J, Ma X M, Li J, Mao R S, Yuan Y J, Wu B, Sheng L N, Yang J C, Xu H S, Zhu L F and Ma X 2018 *Astrophys. J. Suppl. Ser.* **235** 2

[43] Huang Z K, Wen W Q, Xu X, Wang S X, Wang H B, Dou L J, Mahmood S, Khan N, Xu W Q, Xu T H, Yao K, Chuai X Y, Zhu X L, Zhao D M, Mao L J, Yang J C, Yuan Y J, Zhu L F and Ma X 2018 *J. Phys.: Conf. Ser.* **875** 012020

[44] Fritzsche S 2021 *Astron. Astrophys.* **656** A163

[45] Wang S X, Huang Z K, Wen W Q, Chen C Y, Schippers S, Xu X, Sardar S, Khan N, Wang H B, Dou L J, Mahmood S, Zhao D M, Zhu X L, Mao L J, Ma X M, Li J, Tang M T, Mao R S, Yin D Y, Yuan Y J, Yang J C, Shi Y L, Dong C Z, Ma X W and Zhu L F 2019 *Astron. Astrophys.* **627** A171

[46] Wang S, Huang Z, Wen W, Ma W, Wang H, Schippers S, Wu Z, Kozhedub Y, Kaygorodov M and Volotka A 2022 arXiv: 2205.01334

[47] Khan N, Huang Z K, Wen W Q, Wang S X, Chen C Y, Zhang C Y, Wang H B, Liu X, Ma W L, Chen D Y, Yao K, Zhao D M, Mao L J, Ma X M, Li J, Tang M T, Yin D Y, Yuan Y J, Yang J C, Zhu L F and Ma X W 2022 *J. Phys. B: At., Mol. Opt. Phys.* **55** 035001

[48] Mahmood S, Huang Z K, Wen W Q, Wang S X, Chen C Y, Khan N, Xu X, Dou L J, Wang H B, Zhu X L, Zhao D M, Mao L J, Ma X M, Li J, Tang M T, Mao R S, Yang W Q, Yin D Y, Yuan Y J, Yang J C, Zhu L F and Ma X 2020 *J. Phys. B: At., Mol. Opt. Phys.* **53** 085004

[49] Wen W Q, Huang Z K, Wang S X, Khan N, Wang H B, Chen C Y, Zhang C Y, Preval S, Badnell N R, Ma W L, Chen D Y, Liu X, Zhao D M, Mao L J, Li J, Ma X M, Tang M T, Yin D Y, Yang W Q, Yuan Y J, Yang J C, Zhu L F and Ma X 2020 *Astrophys. J.* **905** 36

[50] Yang J C, Xia J W, Xiao G Q, Xu H S, Zhao H W, Zhou X H, Ma X W, He Y, Ma L Z, Gao D Q, Meng J, Xu Z, Mao R S, Zhang W, Wang Y Y, Sun L T, Yuan Y J, Yuan P, Zhan W L, Shi J, Chai W P, Yin D Y, Li P, Li J, Mao L J, Zhang J Q and Sheng L N 2013 *Nucl. Instrum. Method B* **317** 263

[51] Huang Z K, Wen W Q, Xu X, Wang H B, Dou L J, Chuai X Y, Zhu X L, Zhao D M, Li J, Ma X M, Mao L J, Yang J C, Yuan Y J, Xu W Q, Xie L Y, Xu T H, Yao K, Dong C Z, Zhu L F and Ma X 2017 *Nucl. Instrum. Method B* **408** 135

[52] Ma X, Wen W Q, Zhang S F, Yu D Y, Cheng R, Yang J, Huang Z K, Wang H B, Zhu X L, Cai X, Zhao Y T, Mao L J, Yang J C, Zhou X H, Xu H S, Yuan Y J, Xia J W, Zhao H W, Xiao G Q and Zhan W L 2017 *Nucl. Instrum. Method B* **408** 169

[53] Knapp D A, Marrs R E, Levine M A, Bennett C L, Chen M H, Henderson J R, Schneider M B and Scofield J H 1989 *Phys. Rev. Lett.* **62** 2104

[54] Ali R, Bhalla C P, Cocke C L and Stockli M 1990 *Phys. Rev. Lett.* **64** 633

[55] O'Rourke B E, Kuramoto H, Li Y M, Ohtani S, Tong X M, Watanabe H and Currell F J 2004 *J. Phys. B: At., Mol. Opt. Phys.* **37** 2343

[56] Beiersdorfer P, Phillips T W, Wong K L, Marrs R E and Vogel D A 1992 *Phys. Rev. A* **46** 3812

[57] Zhang X, López-Urrutia J R C, Guo P, Mironov V, Shi X, Martínez A J G, Tawara H and Ullrich J 2004 *J. Phys. B: At., Mol. Opt. Phys.* **37** 2277

[58] Shah C, Jörg H, Bernitt S, Dobrodey S, Steinbrügge R, Beilmann C, Amaro P, Hu Z, Weber S, Fritzsche S, Surzhykov A, Crespo López-Urrutia J R and Tashenov S 2015 *Phys. Rev. A* **92** 042702

[59] Knapp D A, Marrs R E, Schneider M B, Chen M H, Levine M A and Lee P 1993 *Phys. Rev. A* **47** 2039

[60] Watanabe H, Tobiyama H, Kavanagh A P, Li Y M, Nakamura N, Sakaue H A, Currell F J and Ohtani S 2007 *Phys. Rev. A* **75** 012702

[61] Yao K, Geng Z, Xiao J, Yang Y, Chen C, Fu Y, Lu D, Hutton R and Zou Y 2010 *Phys. Rev. A* **81** 022714

[62] Tu B, Xiao J, Shen Y, Yang Y, Lu D, Xu T H, Li W X, Chen C Y, Fu Y, Wei B, Zheng C, Huang L Y, Hutton R, Wang X, Yao K, Zou Y, Zhang B H and Tang Y J 2016 *Phys. Plasmas* **23** 053301

[63] Harman Z, Shah C, González Martínez A J, Jentschura U D, Tawara H, Keitel C H, Ullrich J and Crespo López-Urrutia J R 2019 *Phys. Rev. A* **99** 012506

[64] Xiong G, Zhang J, Hu Z, Nakamura N, Li Y, Han X, Yang J and Zhang B 2013 *Phys. Rev. A* **88** 042704

[65] DeWitt D R, Schneider D, Clark M W, Chen M H and Church D 1991 *Phys. Rev. A* **44** 7185

[66] O'Rourke B E, Currell F J, Kuramoto H, Ohtani S, Watanabe H, Li Y M, Tawara T and Tong X M 2008 *Phys. Rev. A* **77** 062709

[67] Hu Z, Li Y and Nakamura N 2013 *Phys. Rev. A* **87** 052706

[68] Nakamura N, Kavanagh A P, Watanabe H, Sakaue H A, Li Y, Kato D, Currell F J and Ohtani S 2008 *Phys. Rev. Lett.* **100** 073203

[69] González Martínez A J, López-Urrutia J R C, Braun J, Brenner G, Bruhns H, Lapierre A, Mironov V, Soria Orts R, Tawara H, Trinczek M, Ullrich J and Scofield J H 2005 *Phys. Rev. Lett.* **94** 203201

[70] Hu Z, Xiong G, He Z, Yang Z, Numadate N, Huang C, Yang J, Yao K, Wei B, Zou Y, Wu C, Ma Y, Wu Y, Gao X and Nakamura N 2022 *Phys. Rev. A* **105** L030801

[71] Tong X M, Hu Z, Li Y, Han X, Kato D, Watanabe H and Nakamura N 2015 *J. Phys. B: At., Mol. Opt. Phys.* **48** 144002

[72] Beilmann C, Mokler P H, Bernitt S, Keitel C H, Ullrich J, Lopez-Urrutia J R and Harman Z 2011 *Phys. Rev. Lett.* **107** 143201

[73] Schnell M, Gwinner G, Badnell N R, Bannister M E, Böhm S, Colgan J, Kieslich S, Loch S D, Mitnik D, Müller A, Pindzola M S, Schippers S, Schwalm D, Shi W, Wolf A and Zhou S G 2003 *Phys. Rev. Lett.* **91** 043001

[74] Beilmann C, Harman Z, Mokler P H, Bernitt S, Keitel C H, Ullrich J and López-Urrutia J R C 2013 *Phys. Rev. A* **88** 062706

[75] Beilmann C, Postavaru O, Arntzen L H, Ginzel R, Keitel C H, Mäckel V, Mokler P H, Simon M C, Tawara H, Tupitsyn I I, Ullrich J, Crespo López-Urrutia J R and Harman Z 2009 *Phys. Rev. A* **80** 050702

[76] Chantler C T, Kinnane M N, Gillaspy J D, Hudson L T, Payne A T, Smale L F, Henins A, Pomeroy J M, Tan J N, Kimpton J A, Takacs E and Makonyi K 2012 *Phys. Rev. Lett.* **109** 153001

[77] Kubiček K, Mokler P H, Mäckel V, Ullrich J and López-Urrutia J R C 2014 *Phys. Rev. A* **90** 032508

[78] Chantler C T, Payne A T, Gillaspy J D, Hudson L T, Smale L F, Henins A, Kimpton J A and Takacs E 2014 *New J. Phys.* **16** 123037

[79] Epp S W, Steinbrügge R, Bernitt S, Rudolph J K, Beilmann C, Bekker H, Müller A, Versolato O O, Wille H C, Yavaş H, Ullrich J and Crespo López-Urrutia J R 2015 *Phys. Rev. A* **92** 020502

[80] Beiersdorfer P, Osterheld A L, Scofield J H, Crespo López-Urrutia J R and Widmann K 1998 *Phys. Rev. Lett.* **80** 3022

[81] O'Neil G, Sanders S, Szypryt P, Dipti, Gall A, Yang Y, Brewer S M, Doriese R, Fowler J, Naing A, Swetz D, Tan J, Ullom J, Volotka A V, Takacs E and Ralchenko Y 2020 *Phys. Rev. A* **102** 032803

[82] Beiersdorfer P, Chen H, Thorn D B and Trabert E 2005 *Phys. Rev. Lett.* **95** 233003

[83] Rzadkiewicz J, Yang Y, Kozioł K, O'Mullane M G, Patel A, Xiao J, Yao K, Shen Y, Lu D, Hutton R, Zou Y and Contributors J E T 2018 *Phys. Rev. A* **97** 052501

[84] Gillaspy J D, Lin T, Tedesco L, Tan J N, Pomeroy J M, Laming J M, Brickhouse N, Chen G X and Silver E 2011 *Astrophys. J.* **728** 132

[85] Nakamura N, Numadate N, Kono Y, Murakami I, Kato D, Sakaue H A and Hara H 2021 *Astrophys. J.* **921** 115

[86] Clementson J, Beiersdorfer P and Gu M F 2010 *Phys. Rev. A* **81** 012505

[87] Qiu M L, Zhao R F, Guo X L, Zhao Z Z, Li W X, Du S Y, Xiao J, Yao K, Chen C Y, Hutton R and Zou Y 2014 *J. Phys. B: At., Mol. Opt. Phys.* **47** 175002

[88] Ralchenko Y, Draganić I N, Osin D, Gillaspy J D and Reader J 2011 *Phys. Rev. A* **83** 032517

[89] Das T, Podpaly Y A, Reader J, Gillaspy J D and Ralchenko Y 2018 *Eur. Phys. J. D* **72** 124

[90] Lu D, Yang Y, Xiao J, Shen Y, Fu Y, Wei B, Yao K, Hutton R and Zou Y 2014 *Rev. Sci. Instrum.* **85** 093301

[91] Li W, Grumer J, Yang Y, Brage T, Yao K, Chen C, Watanabe T, Jönsson P, Lundstedt H, Roger H and Zou Y 2015 *Astrophys. J.* **807** 69

[92] Chen W D, Hu W, Fu Y Q, Xiao J, Liu Y, Meng F C, Shen T M, Chen C Y, Wu S, Wei B, Hutton R and Zou Y 2007 *Phys. Plasmas* **14** 103302

[93] Fritzsche S, Surzhykov A and Stöhlker T 2009 *Phys. Rev. Lett.* **103** 113001

[94] Hu Z, Han X, Li Y, Kato D, Tong X and Nakamura N 2012 *Phys. Rev. Lett.* **108** 073002

[95] Jörg H, Hu Z, Bekker H, Blessenohl M A, Hollain D, Fritzsche S, Surzhykov A, Crespo López-Urrutia J R and Tashenov S 2015 *Phys. Rev. A* **91** 042705

[96] Amaro P, Shah C, Steinbrügge R, Beilmann C, Bernitt S, López-Urrutia J R C and Tashenov S 2017 *Phys. Rev. A* **95** 022712

[97] Shah C, Amaro P, Steinbrügge R, Beilmann C, Bernitt S, Fritzsche S, Surzhykov A, Crespo López-Urrutia J R and Tashenov S 2016 *Phys. Rev. E* **93** 061201

[98] Shah C, Amaro P, Steinbrügge R, Bernitt S, López-Urrutia J R C and Tashenov S 2018 *Astrophys. J. Suppl. Ser.* **234** 27

[99] Kozlov M G, Safronova M S, Crespo López-Urrutia J R and Schmidt P O 2018 *Rev. Mod. Phys.* **90** 045005

[100] Schmöger L, Versolato O O, Schwarz M, Kohnen M, Windberger A, Piest B, Baumann S Feuchtenbeiner, Pedregosa-Gutierrez J, Leopold T, Micke P, Hansen A K, Baumann T M, Drewsen M, Ullrich J, Schmidt P O and López-Urrutia J R C 2015 *Science* **347** 1233

[101] Micke P, Leopold T, King S A, Benkler E, Spieß L J, Schmöger L, Schwarz M, Crespo López-Urrutia J R and Schmidt P O 2020 *Nature* **578** 60

[102] Liu X, Zhou X P, Wen W Q, Lu Q F, Yan C L, Xu G Q, Xiao J, Volotka A V, Kozhedub Y S, Kaygorodov M Y, Huang Z K, Ma W L, Wang S X and Ma X 2021 *Phys. Rev. A* **104** 062804

[103] Parthey C G, Matveev A, Alnis J, Bernhardt B, Beyer A, Holzwarth R, Maistrou A, Pohl R, Predehl K, Udem T, Wilken T, Kolachevsky N, Abgrall M, Rovera D, Salomon C, Laurent P and Hänsch T W 2011 *Phys. Rev. Lett.* **107** 203001

[104] Brandt A D, Cooper S F, Rasor C, Burkley Z, Matveev A and Yost D C 2022 *Phys. Rev. Lett.* **128** 023001

[105] Bezginov N, Valdez T, Horbatsch M, Marsman A, Vutha A C and Hessels E A 2019 *Science* **365** 1007

[106] Glazov D A, Köhler-Langes F, Volotka A V, Blaum K, Heiße F, Plunien G, Quint W, Rau S, Shabaev V M, Sturm S and Werth G 2019 *Phys. Rev. Lett.* **123** 173001

[107] Mohr P J, Plunien G and Soff G 1998 *Phys. Rep.* **293** 227

[108] Safronova M S, Budker D, DeMille D, Kimball D F J, Derevianko A and Clark C W 2018 *Rev. Mod. Phys.* **90** 025008

[109] Stöhlker T, Mokler P H, Bosch F, Dunford R W, Franzke F, Klepper O, Kozhuharov C, Ludziejewski T, Nolden F, Reich H, Rymuza P, Stachura Z, Steck M, Swiat P and Warczak A 2000 *Phys. Rev. Lett.* **85** 3109

[110] Xia J W, Zhan W L, Wei B W, Yuan Y J, Song M T, Zhang W Z, Yang X D, Yuan P, Gao D Q, Zhao H W, Yang X T, Xiao G Q, Man K T, Dang J R, Cai X H, Wang Y F, Tang J Y, Qiao W M, Rao Y N, He Y, Mao L Z and Zhou Z Z 2002 *Nucl. Instrum. Method A* **488** 11

[111] Shabaev V M 2002 *Phys. Rep.* **356** 119

[112] Gumberidze A, Stöhlker T, Banaś D, Beckert K, Beller P, Beyer H F, Bosch F, Hagmann S, Kozhuharov C, Liesen D, Nolden F, Ma X, Mokler P H, Steck M, Sierpowski D and Tashenov S 2005 *Phys. Rev. Lett.* **94** 223001

[113] Gassner T, Trassinelli M, Heß R, Spillmann U, Banaś D, Blumenhagen K H, Bosch F, Brandau C, Chen W, Dimopoulou C, Förster E, Grisenti R E, Gumberidze A, Hagmann S, Hillenbrand P M, Indelicato P, Jagodzinski P, Kämpfer T, Kozhuharov C, Lestinsky M, Liesen D, Litvinov Y A, Loetzsch R, Manil B, Märtin R, Nolden F, Petridis N, Sanjari M S, Schulze K S, Schwemlein M, Simionovici A, Steck M, Stöhlker T, Szabo C I, Trotsenko S, Uschmann I, Weber G, Wehrhan O, Winckler N, Winters D F A, Winters N, Ziegler E and Beyer H F 2018 *New J. Phys.* **20** 073033

[114] Kraft-Bermuth S, Andrianov V, Bleile A, Echler A, Egelhof P, Grabitz P, Ilieva S, Kiselev O, Kilbourne C, McCammon D, Meier J P and Scholz P 2017 *J. Phys. B: At., Mol. Opt. Phys.* **50** 055603

[115] Yerokhin V A and Shabaev V M 2015 *J. Phys. Chem. Ref. Data* **44** 033103

[116] Beiersdorfer P 2010 *J. Phys. B: At., Mol. Opt. Phys.* **43** 074032

[117] Indelicato P 2019 *J. Phys. B: At., Mol. Opt. Phys.* **52** 232001

[118] Beier T, Beinker M, Persson E, Zschocke S and Soff G 1998 *Hyperfine Interact.* **114** 3

[119] Ullmann J, Andelkovic Z, Brandau C, Dax A, Geithner W, Geppert C, Gorges C, Hammen M, Hannen V, Kaufmann S, Konig K, Litvinov Y A, Lochmann M, Maass B, Meisner J, Murbock T, Sanchez R, Schmidt M, Schmidt S, Steck M, Stohlker T, Thompson R C, Trageser C, Vollbrecht J, Weinheimer C and Nortershauser W 2017 *Nat. Commun.* **8** 15484

[120] Huang Z K, Wang S X, Wen W Q, Xu X, Wang H B, Li S, Dou L J, Khan N, Mahmood S, Zhu X L, Zhao D M, Mao L J, Ma X M, Li J, Mao R S, Yang J C, Yin D Y, Yuan Y J, Chen C Y, Zhu L F and Ma X 2020 *X-Ray Spectrometry* **49** 155

[121] Schippers S 2012 *J. Phys. Conf. Ser.* **388** 012010

[122] Savin D W 2007 *J. Phys. Conf. Ser.* **388** 012071

[123] Preval S, Badnell N and O'Mullane M 2017 *AIP Conf. Proc.* **1811** 030002

[124] Badnell N, Spruck K, Krantz C, Novotny O, Becker A, Bernhardt D, Grieser M, Hahn M, Repnow R and Savin D W 2016 *Phys. Rev. A* **93** 052703

[125] Preval S, Badnell N and O'Mullane M 2016 *Phys. Rev. A* **93** 042703

[126] Preval S, Badnell N and O'Mullane M 2017 *J. Phys. B: At., Mol. Opt. Phys.* **50** 105201

[127] Preval S P, Badnell N R and O'Mullane M 2018 *J. Phys. B: At., Mol. Opt. Phys.* **51** 045004

[128] Gu M F 2003 *Astrophys. J.* **590** 1131

[129] Colgan J, Pindzola M S, Whiteford A D and Badnell N R 2003 *Astronomy & Astrophysics* **412** 597

[130] Ma X, Zhu X, Liu H, Li B, Zhang S, Cao S, Feng W and Xu S 2008 *Sci. China Phys. Mech.* **51** 755

[131] Flechard X, Nguyen H, Wells E, Ben-Itzhak I and DePaola B D 2001 *Phys. Rev. Lett.* **87** 123203

[132] Lee T G, Nguyen H, Flechard X, DePaola B D and Lin C D 2002 *Phys. Rev. A* **66** 042701

[133] Ma X, Zhang R T, Zhang S F, Zhu X L, Feng W T, Guo D L, Li B, Liu H P, Li C Y, Wang J G, Yan S C, Zhang P J and Wang Q 2011 *Phys. Rev. A* **83** 052707

[134] Dörner R, Mergel V, Spielberger L, Jagutzki O, Unverzagt M, Schmitt W, Ullrich J, Moshammer R, Khemliche H, Prior M, Olson R E, Zhaoyuan L, Wu W, Cocke C L and Schmidt-Böcking H 1996 *AIP Conf. Proc.* **360** 495

[135] Cassimi A, Duponchel S, Flechard X, Jardin P, Sortais P, Hennecart D and Olson R E 1996 *Phys. Rev. Lett.* **76** 3679

[136] Fléchard X, Harel C, Jouin H, Pons B, Adoui L, Frémont F, Cassimi A and Hennecart D 2001 *J. Phys. B: At., Mol. Opt. Phys.* **34** 2759

[137] Guo D L, Ma X, Zhang S F, Zhu X L, Feng W T, Zhang R T, Li B, Liu H P, Yan S C, Zhang P J and Wang Q 2012 *Phys. Rev. A* **86** 052707

[138] Schöffler M S, Titze J N, Schmidt L P H, Jahnke T, Jagutzki O, Schmidt-Böcking H and Dörner R 2009 *Phys. Rev. A* **80** 042702

[139] Schöffler M S, Titze J, Schmidt L P H, Jahnke T, Neumann N, Jagutzki O, Schmidt-Böcking H, Dörner R and Mančev I 2009 *Phys. Rev. A* **79** 064701

[140] Kim H K, Schöffler M S, Houamer S, Chuluunbaatar O, Titze J N, Schmidt L P H, Jahnke T, Schmidt-Böcking H, Galstyan A, Popov Y V and Dörner R 2012 *Phys. Rev. A* **85** 022707

[141] Fischer D, Feuerstein B, DuBois R D, Moshammer R, Lopez-Urrutia J R C, Draganic I, Lorch H, Perumal A N and Ullrich J 2002 *J. Phys. B: At., Mol. Opt. Phys.* **35** 1369

[142] Beiersdorfer P, Boyce K R, Brown G V, Chen H, Kahn S M, Kelley R L, May M, Olson R E, Porter F S, Stahle C K and Tillotson W A 2003 *Science* **300** 1558

[143] Xu J W, Xu C X, Zhang R T, Zhu X L, Feng W T, Gu L, Liang G Y, Guo D L, Gao Y, Zhao D M, Zhang S F, Su M G and Ma X 2021 *Astrophys. J. Suppl. Ser.* **253** 13

[144] Zhang R T, Wulf D, McCammon D, Seely D G, Andrianarijaona V M and Havener C C 2019 *AIP Conf. Proc.* **2160** 070004

[145] Han J, Wei L, Wang B, Ren B, Yu W, Zhang Y, Zou Y, Chen L, Xiao J and Wei B 2021 *Astrophys. J. Suppl. Ser.* **253** 6

[146] Gu L, Kaastra J and Raassen A J J 2016 *Astron. Astrophys. 588* A52

[147] Arnaud K A, Dorman B and Gordon C A 1999 *XSPEC: An X-ray Spectral Fitting Package*

[148] Smith R K, Foster A R, Edgar R J and Brickhouse N S 2014 *Astrophys. J.* **787** 77

[149] Schultz D R, Stancil P C and Rakovic M J 2001 *J. Phys. B: At., Mol. Opt. Phys.* **34** 2739

[150] Mancev I, Mergel V and Schmidt L 2003 *J. Phys. B: At., Mol. Opt. Phys.* **36** 2733

[151] Abufager P N, Fainstein P D, Martínez A E and Rivarola R D 2004 *J. Phys. B: At., Mol. Opt. Phys.* **38** 11

[152] Knoop S, Olson R E and Ott H 2005 *J. Phys. B: At., Mol. Opt. Phys.* **38** 1987

[153] Mančev I and Milojević N 2010 *Phys. Rev. A* **81** 022710

[154] Gao J W, Wu Y, Wang J G, Dubois A and Sisourat N 2019 *Phys. Rev. Lett.* **122** 093402

[155] Guo D L, Gao J W, Zhang S F, Zhu X L, Gao Y, Zhao D M, Zhang R T, Wu Y, Wang J G, Dubois A and Ma X 2021 *Phys. Rev. A* **103** 032827

[156] Knoop S, Fischer D, Xue Y, Zapukhlyak M, Osborne C J, Ergler T, Ferger T, Braun J, Brenner G, Bruhns H, Dimopoulou C, Epp S W, Martínez A J G, Sikler G, Orts R S, Tawara H, Kirchner T, López-Urrutia J R C, Moshammer R, Ullrich J and Hoekstra R 2008 *J. Phys. B: At., Mol. Opt. Phys.* **41** 195203

[157] Zhang R T, Zhu X L, Li X Y, Liu L, Zhang S F, Feng W T, Guo D L, Gao Y, Zhao D M, Wang J G and Ma X 2017 *Phys. Rev. A* **95** 042702

[158] Barany A, Danared H, Cederquist H, Hvelplund P, Knudsen H, Pedersen J O K, Cocke C L, Tunnell L N, Waggoner W and Giese J P 1986 *J. Phys. B: At., Mol. Opt. Phys.* **19** L427

[159] Wang Q, Ma X, Zhu X L and Zhang S F 2011 *J. Phys. B: At., Mol. Opt. Phys.* **45** 025202

[160] Gao R S, Johnson L K, Schafer D A, Newman J H, Smith K A and Stebbings R F 1988 *Phys. Rev. A* **38** 2789

[161] Horsdal E, Jensen B and Nielsen K O 1986 *Phys. Rev. Lett.* **57** 1414

[162] van der Poel M, Nielsen C V, Gearba M A and Andersen N 2001 *Phys. Rev. Lett.* **87** 123201

[163] Fischer D, Gudmundsson M, Berényi Z, Haag N, Johansson H A B, Misra D, Reinhed P, Källberg A, Simonsson A, Støchkel K, Cederquist H and Schmidt H T 2010 *Phys. Rev. A* **81** 012714

[164] Danared H and Barany A 1986 *J. Phys. B: At., Mol. Opt. Phys.* **19** 3109

[165] Agueny H 2015 *Phys. Rev. A* **92** 012702

[166] Guo D, Ma X, Zhang R, Zhang S, Zhu X, Feng W, Gao Y, Hai B, Zhang M and Wang H 2017 *J. Phys.: Conf. Ser.* **875** 092019

[167] Fritsch W and Lin C D 1991 *Phys. Rep.* **202** 1

[168] Ferguson A F and Bates D R 1961 *Proceedings of the Royal Society of London. Series A. Mathematical and Physical Sciences* **264** 540

[169] McCarroll R and Bates D R 1961 *Proceedings of the Royal Society of London. Series A. Mathematical and Physical Sciences* **264** 547

[170] Zygelman B, Cooper D L, Ford M J, Dalgarno A, Gerratt J and Raimondi M 1992 *Phys. Rev. A* **46** 3846

[171] Errea L F, Harel C, Jouini H, Mendez L, Pons B and Riera A 1994 *J. Phys. B: At., Mol. Opt. Phys.* **27** 3603

[172] Bransden B H, McDowell M R C and Mansky E J 1993 *Phys. Today* **46** 124

[173] Sisourat N, Pilskog I and Dubois A 2011 *Phys. Rev. A* **84** 052722

[174] Gao J W, Wu Y and Wang J G 2018 *Phys. Rev. A* **97** 052709

[175] Aumayr F, Ueda K, Sokell E, Schippers S, Sadeghpour H, Merkt F, Gallagher T F, Dunning F B, Scheier P, Echt O, Kirchner T, Fritzsche S, Surzhykov A, Ma X, Rivarola R, Fojon O, Tribedi L, Lamour E, Crespo López-Urrutia J R, Litvinov Y A, Shabaev V, Cederquist H, Zettergren H, Schleberger M, Wilhelm R A, Azuma T, Boduch P, Schmidt H T and Stöhlker T 2019 *J. Phys. B: At., Mol. Opt. Phys.* **52** 171003

[176] Abdurakhmanov I B, Kadyrov A S, Avazbaev S K and Bray I 2016 *J. Phys. B: At., Mol. Opt. Phys.* **49** 115203

[177] Leung A C K and Kirchner T 2019 *Eur. Phys. J. D* **73** 246

[178] Milburn G J, Jacobs K and Walls D F 1994 *Phys. Rev. A* **50** 5256

[179] Winter T G 2007 *Phys. Rev. A* **76** 062702

[180] Liu X J, Liu L, Wang J G, Qu Y Z and Xiao B J 2011 *Phys. Plasmas* **18** 103301

[181] Faulkner J, Abdurakhmanov I B, Alladustov S U, Kadyrov A S and Bray I 2019 *Plasma Phys. Contr. F.* **61** 095005

[182] Brouillard F, Claeys W, Poulaert G, Rahmat G and Wassenhove G V 1979 *J. Phys. B: At., Mol. Opt. Phys.* **12** 1253

[183] Peart B and Forrest R A 1979 *J. Phys. B: At., Mol. Opt. Phys.* **12** L23

[184] Shingal R and Bransden B H 1990 *J. Phys. B: At., Mol. Opt. Phys.* **23** 1203

[185] Wang J, Hansen J P and Dubois A 2000 *J. Phys. B: At., Mol. Opt. Phys.* **33** 241

[186] Bräuning H, Helm H, Briggs J S and Salzborn E 2007 *Phys. Rev. Lett.* **99** 173202

[187] Stenrup M, Larson Å and Elander N 2009 *Phys. Rev. A* **79** 012713

[188] Mezei J Z, Stenrup M, Elander N and Larson Å 2010 *Phys. Rev. A* **82** 014701

[189] Yan L L, Wu Y, Qu Y Z, Wang J G and Buenker R J 2013 *Phys. Rev. A* **88** 022706

[190] Dubois A, Nielsen S E and Hansen J P 1993 *J. Phys. B: At., Mol. Opt. Phys.* **26** 705

[191] Ghanbari-Adivi E and Ghavaminia H 2012 *Eur. Phys. J. D* **66** 318
[192] Amaldi U and Kraft G 2005 *Rep. Prog. Phys.* **68** 1861
[193] Belkić D 2010 *J. Math. Chem.* **47** 1366
[194] Janev R 2005 *Contem. Phys.* **46** 121
[195] Delabie E, Brix M, Giroud C, Jaspers R J E, Marchuk O, O'Mullane M G, Ralchenko Y, Surrey E, von Hellermann M G and Zastrow K D 2010 *Plasma Phys. Contr. F.* **52** 125008
[196] Cravens T E 2002 *Science* **296** 1042
[197] Voitkiv A B 2004 *Phys. Rep.* **392** 191
[198] Anholt R and Gould H 1986 *Adv. Atom. Mol. Phys.* **22** 315
[199] Bertulani C A and Baur G 1988 *Phys. Rep.* **163** 299
[200] Eichler J 1990 *Phys. Rep.* **193** 165
[201] Najjari A B V B and Ullrich J 2008 *Phys. Rev. Lett.* **101** 223201
[202] Voitkiv A B and Najjari B 2005 *J. Phys. B: At., Mol. Opt. Phys.* **38** 3587
[203] Neumann N, Hant D, Schmidt L P H, Titze J, Jahnke T, Czasch A, Schöffler M S, Kreidi K, Jagutzki O, Schmidt-Böcking H and Dörner R 2010 *Phys. Rev. Lett.* **104** 103201
[204] Khan A, Tribedi L C and Misra D 2017 *Phys. Rev. A* **96** 012703
[205] Wang B, Han J, Zhu X, Wei L, Ren B, Zhang Y, Yu W, Yan S, Ma X, Zou Y, Chen L and Wei B 2021 *Phys. Rev. A* **103** 042810
[206] Xu S, Zhu X L, Feng W T, Guo D L, Zhao Q, Yan S, Zhang P, Zhao D M, Gao Y, Zhang S F, Yang J and Ma X 2018 *Phys. Rev. A* **97** 062701
[207] Jiang T, Wang B, Zhang Y, Wei L, Chen S, Yu W, Zou Y, Chen L and Wei B 2019 *Phys. Rev. A* **100** 022705
[208] Ren B, Xia Z, Zhang Y, Wei L, Yu W, Han J, Wang B, Zou Y, Chen L and Wei B 2021 *Phys. Rev. A* **104** 022811
[209] Ma C, Xu S, Zhao D, Guo D, Yan S, Feng W, Zhu X and Ma X 2020 *Phys. Rev. A* **101** 052701
[210] Yuan H, Xu Z, Xu S, Ma C, Zhang Z, Guo D, Zhu X, Zhao D, Zhang S, Yan S, Gao Y, Zhang R and Ma X 2022 *Phys. Rev. A* **105** 022814
[211] He Z, Wang J, Zhang Y, Wang B, Han J, Ren B, Wei L, Xia Z, Ma P, Meng T, Zou Y, Hu Z and Wei B 2022 *Phys. Rev. A* **105** 022818
[212] Jana M R, Ghosh P N, Bapat B, Kushawaha R K, Saha K, Prajapati I A and Safvan C P 2011 *Phys. Rev. A* **84** 062715
[213] Zhang Y, Jiang T, Wei L, Luo D, Wang X, Yu W, Hutton R, Zou Y and Wei B 2018 *Phys. Rev. A* **97** 022703
[214] Khan A, Tribedi L C and Misra D 2015 *Phys. Rev. A* **92** 030701
[215] Maclot S, Delaunay R, Piekarski D G, Domaracka A, Huber B A, Adoui L, Martín F, Alcamí M, Avaldi L, Bolognesi P, Díaz-Tendero S and Rousseau P 2016 *Phys. Rev. Lett.* **117** 073201
[216] Maclot S, Piekarski D G, Delaunay R, Domaracka A, Méry A, Vizcaino V, Chesnel J Y, Martín F, Alcamí M, Huber B A, Adoui L, Rousseau P and Díaz-Tendero S 2014 *Eur. Phys. J. D* **68** 149
[217] Maclot S, Piekarski D G, Domaracka A, Méry A, Vizcaino V, Adoui L, Martín F, Alcamí M, Huber B A, Rousseau P and Díaz-Tendero S 2013 *J. Phys. Chem. Lett.* **4** 3903
[218] Piekarski D G, Delaunay R, Maclot S, Adoui L, Martín F, Alcamí M, Huber B A, Rousseau P, Domaracka A and Díaz-Tendero S 2015 *Phys. Chem. Chem. Phys.* **17** 16767
[219] Piekarski D G, Delaunay R, Mika A, Maclot S, Adoui L, Martín F, Alcamí M, Huber B A, Rousseau P and Díaz-Tendero S 2017 *Phys. Chem. Chem. Phys.* **19** 19609
[220] Barreiro-Lage D, Nicolafrancesco C, Kočišek J, Luna A, Kopyra J, Alcamí M, Huber B A, Martín F, Domaracka A and Rousseau P 2022 *Phys. Chem. Chem. Phys.* **24** 941
[221] Holm A I, Zettergren H, Johansson H A, Seitz F, Rosen S, Schmidt H T, Ławicki A, Rangama J, Rousseau P and Capron M 2010 *Phys. Rev. Lett.* **105** 213401
[222] Wei L, Ren B, Zhang Y, Wang J, Wang B, Han J, Yu W, Zou Y, Chen L and Wei B 2021 *Phys. Rev. A* **103** 012810
[223] Zhang Y, Ren B, Yang C L, Wei L, Wang B, Han J, Yu W, Qi Y, Zou Y and Chen L 2020 *Commun. Chem.* **3** 1
[224] Wei L, Lam C S, Zhang Y, Ren B, Han J, Wang B, Zou Y, Chen L, Lau K C and Wei B 2021 *J. Phys. Chem. Lett.* **12** 5789
[225] Méry A, Agnihotri A N, Douady J, Fléchard X, Gervais B, Guillous S, Iskandar W, Jacquet E, Matsumoto J, Rangama J, Ropars F, Safvan C P, Shiromaru H, Zanuttini D and Cassimi A 2017 *Phys. Rev. Lett.* **118** 233402
[226] Ding X, Haertelt M, Schlauderer S, Schuurman M S, Naumov A Y, Villeneuve D M, McKellar A R W, Corkum P B and Staudte A 2017 *Phys. Rev. Lett.* **118** 153001
[227] Markush P, Bolognesi P, Cartoni A, Rousseau P, Maclot S, Delaunay R, Domaracka A, Kocisek J, Castrovilli M C, Huber B A and Avaldi L 2016 *Phys. Chem. Chem. Phys.* **18** 16721
[228] Nomura S, Tsuchida H, Kajiwara A, Yoshida S, Majima T and Saito M 2017 *J. Chem. Phys.* **147** 225103
[229] Hu X, Peng Y, Zhu X, Yan S, Liu L, Feng W, Guo D, Gao Y, Zhang S and Zhao D 2020 *Phys. Rev. A* **101** 012707
[230] Peng Y, Hu X, Wu Y, Wang J, Lu R and Sisourat N 2021 *J. Phys. B: At., Mol. Opt. Phys.* **54** 125102
[231] Buenker R J and Peyerimhoff S D 1974 *Theor. Chim. Acta* **35** 33
[232] Hu X, Jia C, Xu T, Wu Y and Wang J 2022 *Phys. Rev. A* **106** 012814
[233] Zhao X, Xu T, Yu X, Ren D, Zhang X, Li X, Ma P, Wang C, Zhang D and Wang Q 2021 *Phys. Rev. A* **103** 053103
[234] Lin K, Hu X, Pan S, Chen F, Ji Q, Zhang W, Li H, Qiang J, Sun F and Gong X 2020 *J. Phys. Chem. Lett.* **11** 3129
[235] Davisson C J 1928 *J. Franklin I.* **205** 597
[236] Tuan T F and Gerjuoy E 1960 *Phys. Rev.* **117** 756
[237] Cheng S, Cocke C L, Frohne V, Kamber E Y, McGuire J H and Wang Y 1993 *Phys. Rev. A* **47** 3923
[238] Misra D, Schmidt H T, Gudmundsson M, Fischer D, Haag N, Johansson H A B, Källberg A, Najjari B, Reinhed P, Schuch R, Schöffler M, Simonsson A, Voitkiv A B and Cederquist H 2009 *Phys. Rev. Lett.* **102** 153201
[239] Schmidt H T, Fischer D, Berenyi Z, Cocke C L, Gudmundsson M, Haag N, Johansson H A B, Källberg A, Levin S B, Reinhed P, Sassenberg U, Schuch R, Simonsson A, Støchkel K and Cederquist H 2008 *Phys. Rev. Lett.* **101** 083201
[240] Schmidt L P H, Schössler S, Afaneh F, Schöffler M, Stiebing K E, Schmidt-Böcking H and Dörner R 2008 *Phys. Rev. Lett.* **101** 173202
[241] Landers A L, Wells E, Osipov T, Carnes K D, Alnaser A S, Tanis J A, McGuire J H, Ben-Itzhak I and Cocke C L 2004 *Phys. Rev. A* **70** 042702
[242] Senftleben A, Pflüger T, Ren X, Al-Hagan O, Najjari B, Madison D, Dorn A and Ullrich J 2010 *J. Phys. B: At., Mol. Opt. Phys.* **43** 081002
[243] Alexander J S, Laforge A C, Hasan A, Machavariani Z S, Ciappina M F, Rivarola R D, Madison D H and Schulz M 2008 *Phys. Rev. A* **78** 060701
[244] Egodapitiya K N, Sharma S, Hasan A, Laforge A C, Madison D H, Moshammer R and Schulz M 2011 *Phys. Rev. Lett.* **106** 153202
[245] Zhang S F, Fischer D, Schulz M, Voitkiv A B, Senftleben A, Dorn A, Ullrich J, Ma X and Moshammer R 2014 *Phys. Rev. Lett.* **112** 023201
[246] Stöhlker T, Beyer H F, Bräuning-Demian A, Brandau C, Gumberidze A, Grisenti R E, Hagmann S, Herfurth F, Kozhuharov C, Kühl T, Liesen D, Litvinov Y, Maertin R, Nörtershäuser W, Kester O, Petridis N, Quint W, Schramm U, Schuch R, Spillmann U, Trotsenko S, Weber G and Winters D 2011 *AIP Conf. Proc.* **1336** 132
[247] Kekelidze V, Kovalenko A, Lednicky R, Matveev V, Meshkov I, Sorin A and Trubnikov G 2013 *Status of NICA project at JINR*, 085
[248] Einstein A, Podolsky B and Rosen N 1935 *Phys. Rev.* **47** 777
[249] Bell J S 1964 *Phys. Physique Fizika* **1** 195
[250] Hensen B, Bernien H, Dréau A E, Reiserer A, Kalb N, Blok M S, Ruitenberg J, Vermeulen R F, Schouten R N and Abellán C 2015 *Nature* **526** 682
[251] Tielens A G G M 2013 *Rev. Mod. Phys.* **85** 1021
[252] Ishak B 2019 *Contemp. Phys.* **60** 262
[253] Seiferle B, von der Wense L, Bilous P V, Amersdorffer I, Lemell C, Libisch F, Stellmer S, Schumm T, Düllmann C E, Pálffy A and Thirolf P G 2019 *Nature* **573** 243
[254] Ma X, Wen W Q, Huang Z K, Wang H B, Yuan Y J, Wang M, Sun Z Y, Mao L J, Yang J C, Xu H S, Xiao G Q and Zhan W L 2015 *Phys. Scr.* **T166** 014012
[255] Hoszowska J, Dousse J C, Szlachetko J, Kayser Y, Cao W, Jagodziński P, Kavčič M and Nowak S 2011 *Phys. Rev. Lett.* **107** 053001
[256] Wölfli W, Stoller C, Bonani G, Suter M and Stöckli M 1975 *Phys. Rev. Lett.* **35** 656
[257] Lyashchenko K N, Andreev O Y and Yu D 2020 *Phys. Rev. A* **101** 040501
[258] Wang Z, Najjari B, Zhang S F, Ma X and Voitkiv A B 2019 *Phys. Rev. A* **100** 052710